Receiver Antenna Separation over Symbol Wavelengths in a MIMO-multiuser UWB System with near LOS Channels

by

V. V. S. Nagesh Polu

B. Tech, Jawaharlal Nehru Technological University, 2004

A THESIS SUBMITTED IN PARTIAL FULFILLMENT OF THE REQUIREMENTS FOR THE DEGREE OF

Master of Science in Engineering

In the Graduate Academic Unit of Electrical and Computer Engineering

Supervisor(s):	Bruce G. Colpitts, B.Sc.E., M.Sc.E., Ph.D.
	Brent R. Petersen, B.Eng., M.A.Sc., Ph.D.
Examining Board:	Maryhelen Stevenson, B.E., M.S., Ph.D.
	Eduardo Castillo Guerra, B.Sc.E., M.Sc.E., Ph.D.
	Balasubramanian Venkatesh, B.E., M.E., Ph.D., Chair
External Examiner:	Bradford G. Nickerson, B.Sc.E., M.Sc.E., Ph.D.

This thesis is accepted

Dean of Graduate Studies

THE UNIVERSITY OF NEW BRUNSWICK

January, 2007

Dedication

To my grandfather, Venkataiah; my grandmother, Budemma; and ammamma, Seetharamamma.

Abstract

This thesis investigates the performance of an ultra-wideband (UWB) multiple-input multiple-output (MIMO) multiuser system with near line-of-sight (LOS) channels. Receiver antenna-element separation on the scale of a symbol wavelength ([speed of light]/[symbol rate]) is proposed. Two different antenna array configurations, a two-element linear array and a three-element triangular array, are used for the receiver. UWB indoor LOS channel measurements were made in the 3 to 7 GHz band for these configurations and included in the simulation. Results show that the three-element triangular array performance is significantly improved over the two-element linear array. It is observed from the experimental results that an optimum receiver antenna-element separation of more than four symbol wavelengths is required for a two-by-two case, whereas three symbol wavelengths is sufficient for a three-by-three case.

Acknowledgements

I have to acknowledge a lot of people who helped me during my graduate study at the University of New Brunswick. First of all, I would like to thank my supervisors Dr. Bruce G. Colpitts and Dr. Brent R. Petersen for giving me the opportunity to work with them. I am greatly thankful for their encouragement and support throughout the course of this research work.

My special thanks to Dr. Rajamani Doraiswami and Dr. Richard Tervo for admitting me to the program. I would also like to acknowledge the cheerful administrative staff: Denise Burke, Shelly Cormier and Karen Annett for their help and guidance, and the technical staff: Kevin Hanscom, Bruce Miller and Blair Allen for helping me with the experimental work. I would especially like to acknowledge Bruce Miller for his prompt assistance in the fabrication of antennas for this work. I would also like to thank my friends for encouraging me even in the hard times. Specifically, I would like to thank Guangran Zhu not only for his suggestions and help in understanding the basics of his work but also for his valuable comments regarding my research work.

This research was generously funded by our industrial partner Aliant Telecom, and the Atlantic Canada Opportunities Agency (ACOA). I would also like to thank David M. Brown of Aliant Telecom for his valuable comments. Last but not the least, I would like to thank my parents, Narasaiah and Vasantha Kumari; my uncle, Byrapaneni Sadasiva Rao; my aunt, Tulasi; and my sisters Madhavi and Latha for their love and support.

Table of Contents

List of Figures

Abbreviations

CCI	Cochannel Interference
FCC	Federal Communications Commission
FSE	Fractionally Spaced Equalizer
GP-IB	General Purpose Interface Bus
HDTV	High Definition Digital Televisions
IEEE	Institute of Electrical and Electronics Engineers
ISI	Inter-symbol Interference
ISM	Industrial Scientific and Medical
LMS	Least Mean Square
LOS	Line-of-Sight
Mbps	Mega bits per second
MIMO	Multiple-Input Multiple-Output
MIMO-MU	Multiple-Input Multiple-Output Multiuser
MISO	Multiple-Input Single-Output
MLSE	Maximum Likelihood Sequence Estimation
MMSE	Minimum Mean Squared Error
MSE	Mean Squared Error
NLOS	Non Line-of-Sight
Rx	Receiver
SIMO	Single-Input Multiple-Output
SISO	Single-Input Single-Output
Tx	Transmitter
UWB	Ultra wideband
VNA	Vector Network Analyzer
VSWR	Voltage Standing Wave Ratio
WLAN	Wireless Local Area Networks
WMAN	Wireless Metropolitan Area Networks
WPAN	Wireless Personal Area Networks
WWAN	Wireless Wide Area Networks

List of Symbols

λ_g	Signalling length or signalling wavelength
λ_T	Symbol wavelength
Δ	Receiver antenna element separation
β	Rolloff factor of the raised cosine filter
ϵ	Mean squared error
$\mathbf{E}[\bullet]$	Expectation operator
σ_d^2	Variance of the users data
$[\bullet]^*$	Denotes complex conjugate
$[\bullet]^H$	Denotes conjugate transpose
$[\bullet]^T$	Denotes transpose
$[\bullet]^{-1}$	Inverse of a matrix
c	Speed of light
d_m	Data from m^{th} user
$\hat{d}_m(k)$	Estimated data for the m^{th} output of the receiver
$e_m(k)$	Error obtained by comparing the received data with the transmitted data
l_{xy}	Distance between the x^{th} transmitter and the y^{th} receiver antenna
L	Number of antenna elements at receiver
M	Number of users
T	Symbol period
$h_{l,m}(t)$	Channel impulse response between m^{th} user and l^{th} receive antenna

$h_{i,l,m}$	Channel impulse response coefficient between m^{th} user and l^{th} receive antenna
$\mathbf{h}_{l,m}$	Channel impulse response matrix between m^{th} user and l^{th} receive antenna
$\mathbf{H}_{ct}(t)$	Overall channel impulse response matrix in continous time
$\mathbf{H}$	Overall channel impulse response matrix in discrete time
$\mathbf{H}_{l,m}$	Channel impulse response convolution matrix for the m^{th} user and the l^{th} receive antenna
$n_c(t)$	Number of channel coefficients
$n_F(t)$	Number of filter coefficients
$n_l(t)$	Noise signal at the antenna element l
$\mathbf{n}(t)$	Noise vector at the L antenna branches
$\mathbf{n}(k)$	Noise vector at the L antenna branches in discrete time
$p(t)$	Time domain response of the raised cosine filter
$P(f)$	Frequency response of the raised cosine filter
$r_l(t)$	Received signal at the antenna element l
$r_l(k)$	Received signal at the antenna element l in the discrete domain
$\mathbf{r}_l(k)$	Received signal vector at the antenna element l in the discrete domain
R_T	Symbol rate
$\mathbf{R}$	Autocorrelation matrix for the received signal vector
$s_m(t)$	Transmitted signal from user m
$\mathbf{s}(t)$	Transmitted signal vector of all users
$\mathbf{s}_m(k)$	Transmitted signal vector of user m in discrete time
$\mathbf{s}(k)$	Transmitted signal vector of all users in discrete time
$w_{i,l,m}$	i^{th} coefficient of the filter between the l^{th} antenna element and the m^{th} output of the linear combiner
$\mathbf{w}_{l,m}$	Filter coefficient vector between the l^{th} antenna element and the m^{th} output of the linear combiner
$\mathbf{W}_m$	Overall filter coefficient vector between the l antenna elements and the m outputs of the linear combiner

Chapter 1

Introduction

The wireless industry is growing at a rapid pace. Due to recent technological developments, wireless networks are providing enhanced services to mobile users at very low cost. Wireless networks are mainly divided into four types: wireless wide area networks (WWAN), wireless metropolitan area networks (WMAN), wireless local area networks (WLAN) and wireless personal area networks (WPAN). The internetworking between these wireless networks provides a continuous service to end-users without losing network connection. With the advent of very large scale integration technology and field-programmable gate arrays, the cost of consumer electronic devices has decreased drastically [1]. This has motivated increased research for indoor wireless applications.

Originally the unlicensed industrial, scientific and medical (ISM) bands were reserved for non-commercial use [2]. In order to meet the demand for wireless connectivity in homes and offices, these ISM bands have been used by the WLAN and WPAN technologies, which are mainly intended for high-speed data transmission. The maximum data rate by a commercial WLAN product achieved to date is 108 Mbps. In order to provide much higher data rates, the IEEE 802.11 task group is trying to develop the IEEE 802.11n WLAN standard, which uses

multiple antennas and can provide data rates above 110 Mbps [3, 4].

Data speeds greater than 100 Mbps are required to connect consumer electronic devices such as high definition digital televisions (HDTV), personal computers, personal digital assistants and digital camcorders, in homes or offices [4]. The high bandwidth requirements of these services are incompatible with the present IEEE 802.11 and Bluetooth standards. Emerging Ultra-Wideband (UWB) technology may be useful to solve these problems.

1.1 Background

This section will provide readers with the background information related to this thesis. It begins by explaining the multiple-input multiple-output (MIMO) technology and its advantages, then it discusses UWB technology and its advantages. Finally it will provide the information on using MIMO technology with UWB.

1.1.1 MIMO Technology

When a signal is transmitted through a wireless channel, it undergoes both amplitude and phase variations by the time it reaches the receiver along with constructive and destructive interference from multipath. Fading is caused by multipath interference that occurs due to reflections/scattering from the nearby objects in the channel. A technique that combines the multiple independent fading paths to overcome the fading effects is called a diversity technique. There are many diversity techniques available, such as frequency diversity, polarization diversity, time diversity and space diversity, of which, space diversity is the most common and is a relatively simple technique. It can be implemented easily by using multiple antennas at the transmitter end or at the receiver end. Due to space constraints, this technique is mainly employed at the basestation receivers.

The antennas must be separated properly to have uncorrelated communication signals. Ideally, they are separated on the scale of a carrier wavelength. The space diversity technique is used not only to combat fading but also to reduce cochannel interference and improve system capacity [5, 6, 7]. Different antenna configurations used in a space-time wireless system are shown in Fig. 1.1. They are Single-Input Single-Output (SISO), Single-Input Multiple-Output (SIMO), Multiple-Input Single-Output (MISO), Multiple-Input Multiple-Output (MIMO) and a MIMO-multi user (MIMO-MU). A MIMO-MU configuration is used in this thesis, in which a base-station with L antenna elements communicates with M users each with one antenna [8].

1.1.2 Ultra wideband Technology

Research in UWB technology began in 1962 [9]. The term 'ultra wideband' was first created by the U.S. Department of Defense in 1989. It has been mainly used for radar applications until now, because of the wideband nature of the signal that results in very accurate timing information. UWB systems use very short duration pulses to transmit data over a large bandwidth, i.e. 7.5 GHz. The Federal Communication Commission (FCC) defines UWB as a signal with either a fractional bandwidth of 20 percent of the center frequency or a minimum of 500 MHz [10].

In 2002, the FCC granted an unlicensed spectrum from 3.1 GHz to 10.6 GHz, at a limited transmit power of -41.3 dBm/MHz as shown in Fig. 1.2 for use in high-speed UWB data services. Currently there are no specific regulations on the UWB spectrum in Canada. Thus, for the research described in this thesis, it was necessary to obtain a developmental license from Industry Canada to perform UWB channel measurements [11]. To allow such a large bandwidth, the FCC put some emission limits so that the existing systems can work effectively

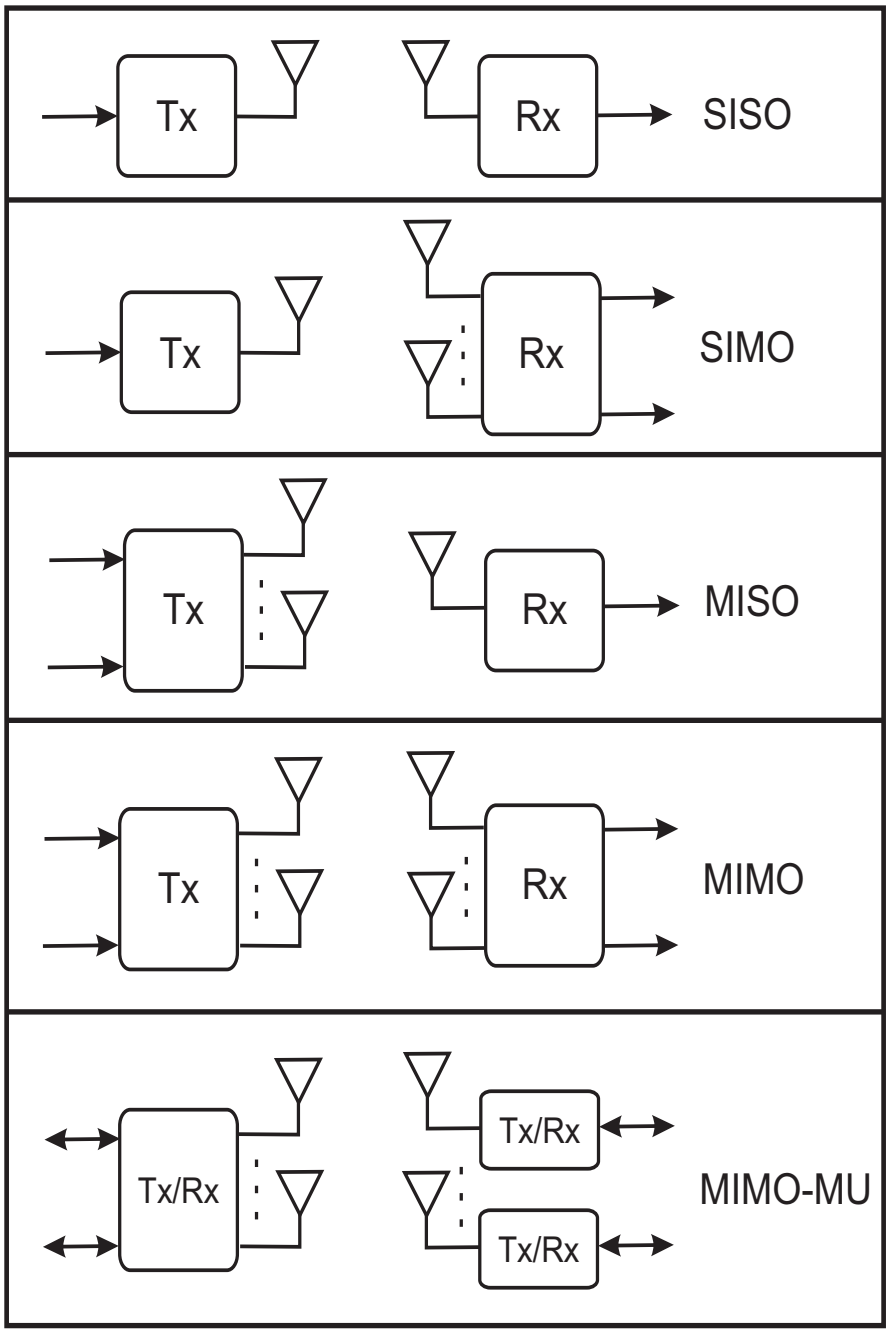

Figure 1.1: Antenna configurations in space-time wireless systems (Tx: Transmitter, Rx: Receiver)[Reproduced from Paulraj et al. [8]]

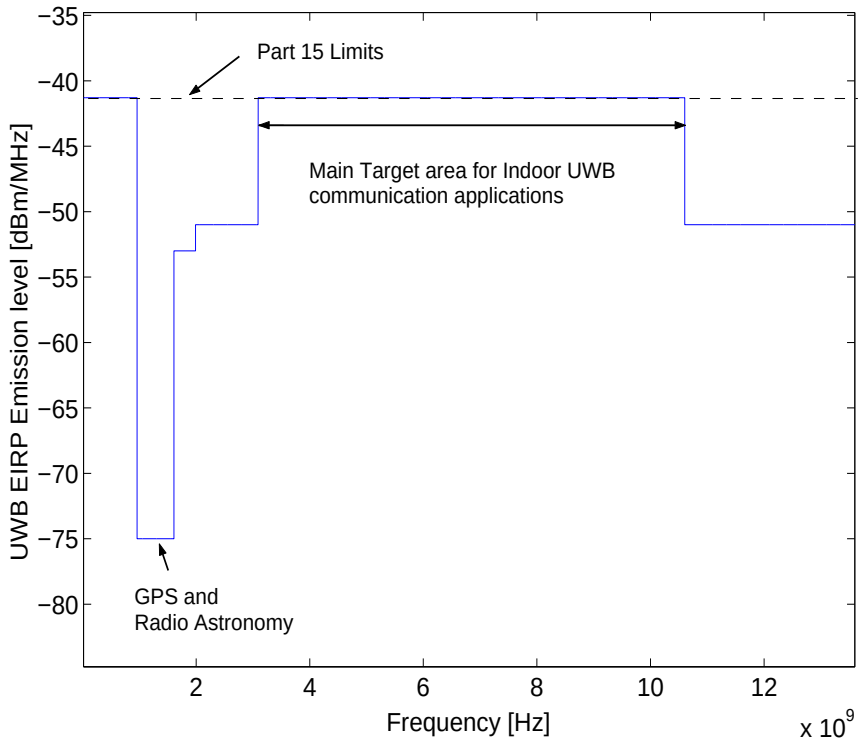

Figure 1.2: Spectral mask mandated by FCC for indoor UWB communications.

without any interference from UWB systems. UWB technology is an efficient solution for the ultra high-speed data services, i.e. speeds up to 480 Mbps, in WPAN environments, i.e. in ranges of 10 m. It is an efficient solution because of its large bandwidth, very simple architecture and low cost. These speeds can be greatly increased by using MIMO techniques.

1.2 Literature Review

UWB systems and the modulation techniques used by this technology have been well known since the 1970s, and until recently have undergone no major developments. After the FCC's allocation of the unlicensed UWB spectrum, research into UWB communications has been renewed, leading to the discovery of more efficient uses of this technology. Despite the advantages offered by this technology, the capabilities of the UWB systems are limited by several challenges such as syn-

chronization, antenna design, spatial diversity, channel estimation and advanced digital signal processing technology [12]. Very little work has been done involving multiple antennas in UWB systems. This thesis concerns the application of multiple antennas to a UWB system. In this thesis, the term: two-by-two case corresponds to two transmitters and two antenna elements at the receiver and the three-by-three case corresponds to three transmitters and three receiver antenna elements.

Important work by Yanikömeroğlu and Sousa [13] shows the dependence of correlated interference on antenna element spacing. They showed that the interference is correlated when the antennas are separated on the scale of carrier wavelength. The authors defined a parameter called chiplength ([speed of light]/[chip rate]), which can be used to separate antennas in a multi antenna system to have uncorrelated interference at the antenna branches and to achieve antenna gain. The work by Roy and Falconer [14] studied the effect of fading correlation on antenna element separation for a local multipoint distribution system operating at 29.5 GHz. They observed significant correlations between signals even when the antenna elements were separated by hundreds of carrier wavelengths.

In LOS pure delay channels, the signals received by the antenna elements separated on the scale of carrier wavelength are almost identical. Thus, there will be no advantage in having multiple antennas. Recently Zhu [15] analyzed the effect of phase in a LOS pure delay channel on achieving spatial multiplexing. He showed that, the receiver antenna elements separated on the scale of signalling length ([speed of light]/[signalling rate]) yielded significant performance improvement. He considered a reverse link scenario in which two transmitters are in communication with a two antenna element receiver as shown in Fig. 1.3(a). The term l_{xy} denotes the distance between the x^{th} transmitter and the y^{th} receiver antenna. Since the path delays incur linear phase differences at the antenna

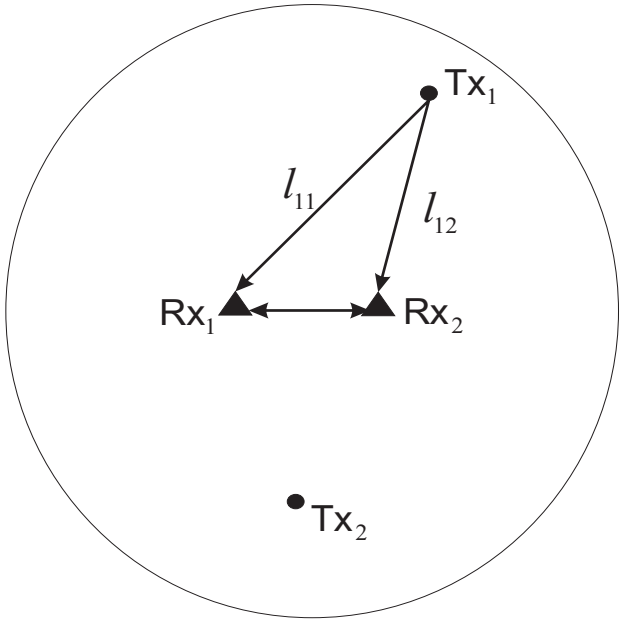

(a)

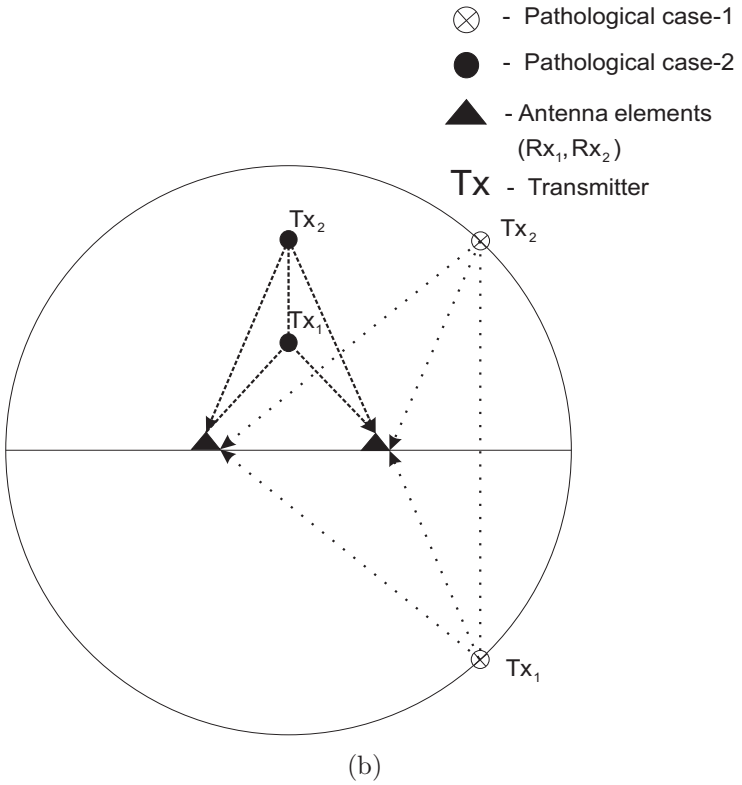

(b)

Figure 1.3: Two-by-two scenario with linear receive antenna elements. (a) General case. (b) Pathological cases.

branches, Zhu first showed that the path lag between the two transmitters at the first receive antenna should be greater than one signalling length

$$|l_{11} - l_{21}| > \lambda_g \tag{1.1}$$

and similarly at the second receive antenna

$$|l_{12} - l_{22}| > \lambda_g \tag{1.2}$$

where λ_g is the signalling length. Since the analysis is only concerned with the delay of the channels, the role of transmitters and receiving antenna elements can be switched. Now the above equations can be written as

$$|l_{11} - l_{12}| > \lambda_g \tag{1.3}$$

and

$$|l_{21} - l_{22}| > \lambda_g. \tag{1.4}$$

The expression in Eq. 1.3 states that, the path lag between the first transmitter to the two receive antennas should be greater than one signalling length and similarly for the second transmitter. In general, the path lags $|l_{11} - l_{12}|$ and $|l_{21} - l_{22}|$ are limited within

$$|l_{11} - l_{12}| < \Delta \tag{1.5}$$

and

$$|l_{21} - l_{22}| < \Delta. \tag{1.6}$$

This gives the final expression

$$\Delta > \lambda_g \tag{1.7}$$

which states that the receiving antenna element separation should be greater than the signalling length.

Zhu also showed that there are certain cases where the two-by-two system fails and named them as pathological cases as shown in Fig. 1.3(b). These pathological cases arise due to the identical slopes of linear phase differences of the two transmitters at the receiver antenna elements.

The aforementioned work motivated our current study on antennas separated on the scale of symbol wavelength. The details regarding symbol-wavelength will be provided in Chapter 2.

1.3 Thesis Contribution

The major contributions of this thesis are listed below.

- This thesis presents the quantification of the antenna-element separation over symbol wavelengths for MMSE-optimized linear multiuser MIMO UWB systems, with near LOS channels.

- Since suitable commercial omnidirectional UWB antennas are not available in the market, we have simulated and fabricated a printed circular disc monopole antenna for measuring UWB MIMO channel impulse responses.

- The performance of an UWB system has been investigated by using mean squared error (MSE) criterion. We have developed a fractionally spaced complex baseband simulation to show the MSE performance.

- Zhu [15] showed the existence of pathological cases in his work. So, we verified the existence of these pathological cases by measuring the UWB

channels for the two-by-two case and have proposed a triangular array at the receiver to mitigate these cases. We also showed the improvement in performance for a three-by-three case compared to the two-by-two case.

1.4 Thesis Organization

The remainder of this thesis is organized as follows

- Chapter 2 gives a brief explanation of the system model and its components, such as transmitter, channel model and the receiver. A linear combiner to detect users jointly and the MSE criterion to optimize the receiver's equalizer is also covered in this chapter.

- Chapter 3 provides a brief explanation of the UWB channel measurement procedure that is used in this thesis. This covers the antenna simulation and fabrication, different channel sounding techniques and the experimental setup used to measure MIMO channels.

- Chapter 4 covers the MATLAB® simulation of both the two-by-two and the three-by-three system models by incorporating the real channel impulse responses. The simulation results of the two models are compared.

- Chapter 5 provides the conclusions of this work and the possibilities of research in the future.

Chapter 2

System model

The objective of this chapter is to give a brief explanation of the UWB MIMO system model and its components. A generalized system model is shown in Fig. 2.1. The main components of the system model are the transmitters[1], wireless channels and the receivers. A multiuser system model with M users and L receiving antenna elements at the receiver is considered with the number of users always equal to the number of receiving antenna elements at the receiver (i. e. $M = L$). The main focus of the system model is the uplink or reverse link scenario where the users, each with a single antenna transmit data to a single base station with multiple receive antennas and multiple outputs. The receiver detects all the users jointly using a MMSE linear combiner.

2.1 Transmitter

The data $d_m(k)$ from user m is a zero-mean unit-variance complex uncorrelated random process, modelling four-point quadrature amplitude modulation. The data takes on the values

[1] In this thesis the term transmitter is a synonym for user.

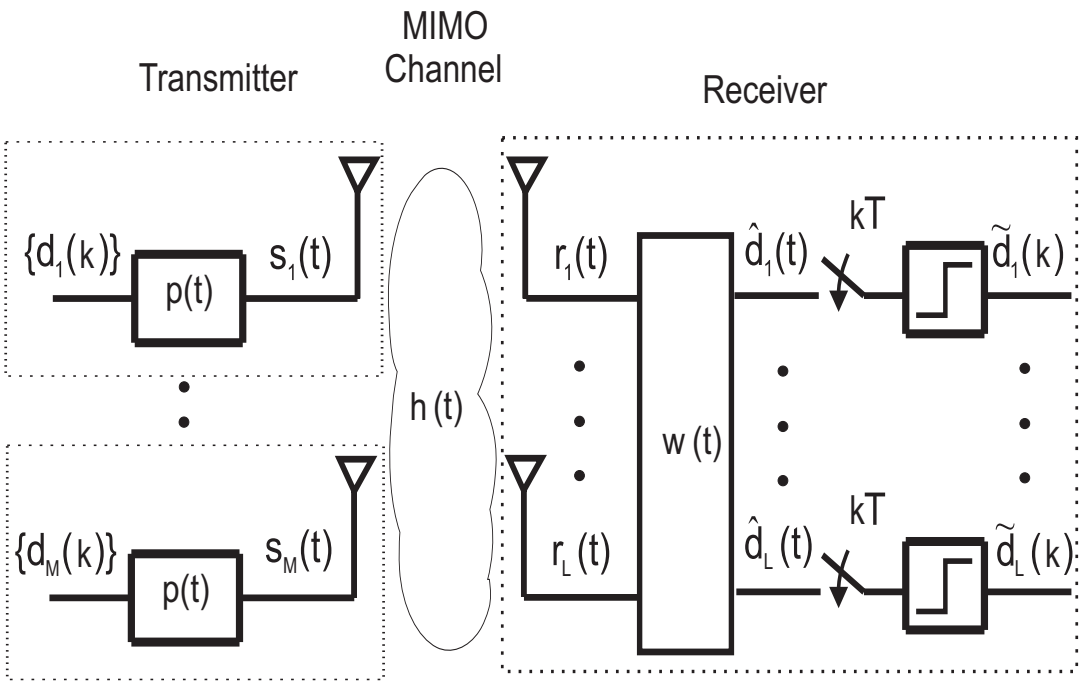

Figure 2.1: Continuous time system model.

$$\{d_m(k)\} \in \frac{1}{\sqrt{2}}\{-1,\, 1,\, -j,\, j\}, \tag{2.1}$$

where $1 \leq m \leq M$,

$$\mathbf{E}[d_m(k)] = 0 \tag{2.2}$$

$$\mathbf{E}[d_m(k)d_m^*(k)] = \sigma_d^2 \tag{2.3}$$

and σ_d^2 is the variance of data equal to one ($\sigma_d^2 = 1$). The symbol $\mathbf{E}[\bullet]$ denotes the expectation operator and * denotes the complex conjugate. This complex data is applied to the input of the $p(t)$ shown in Fig. 2.1.

Pulse shaping is used in digital communication to overcome the effects of interference. A raised cosine pulse shaping filter $p(t)$ with 100 percent excess bandwidth is used for each transmitter. The frequency domain characteristics are given by Gentile [16] and Proakis [17]:

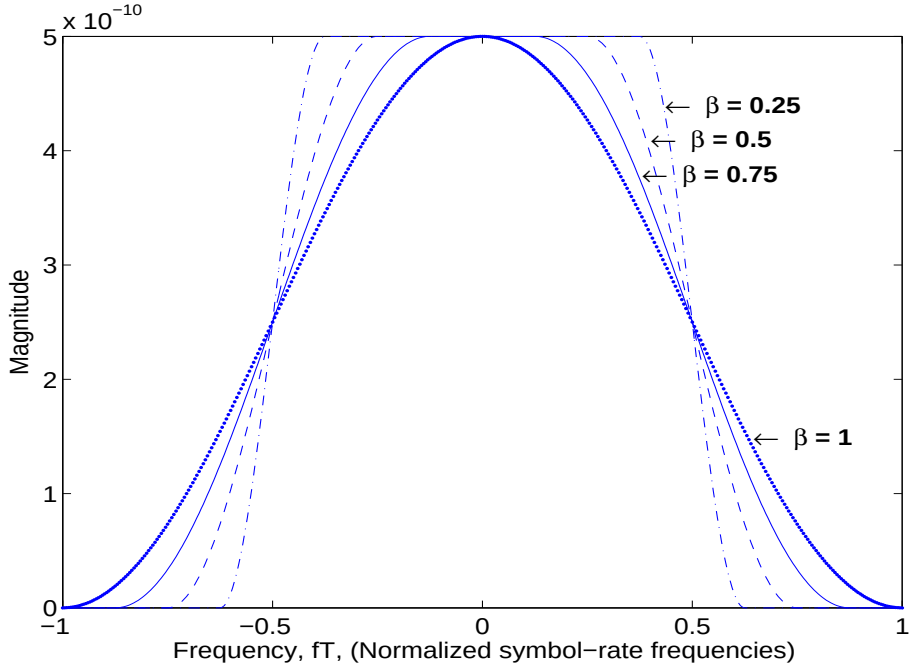

Figure 2.2: Magnitude response of the raised cosine pulse normalized to its symbol rate.

$$P(f) = \begin{cases} T & , \left(0 \leq |f| \leq \frac{1-\beta}{2T}\right) \\ \frac{T}{2}\left\{1 + \cos\left[\frac{\pi T}{\beta}\left(|f| - \frac{1-\beta}{2T}\right)\right]\right\} & , \left(\frac{1-\beta}{2T} \leq |f| \leq \frac{1+\beta}{2T}\right) \\ 0 & , \left(|f| > \frac{1+\beta}{2T}\right) \end{cases} \tag{2.4}$$

where β is the rolloff factor which governs the bandwidth of the transmitted pulse and takes values in the range $0 \leq \beta \leq 1$, T is the symbol period and f is the frequency. The frequency response of this filter is shown in Fig. 2.2. In this thesis, the transmitted data is band limited by the pulse shaping filter, so that it occupies a 4 GHz of bandwidth in both the passband and baseband frequency domains. Thus each symbol occupies a 4 GHz bandwidth. This corresponds to a symbol rate (R_T) of 2 Gsymbols/s at 100 percent excess bandwidth. Therefore, the symbol wavelength (λ_T) is defined as

$$\lambda_T = \frac{c}{R_T} \tag{2.5}$$

where c is the speed of light, to produce

$$\lambda_T = \frac{3 \times 10^8}{2 \times 10^9} \tag{2.6}$$

$$= 0.15 \text{ m}. \tag{2.7}$$

The signal coming out of the raised cosine filter is the convolution of the input and the filter's impulse response, which can be written as

$$s_m(t) = \sum_{n=-\infty}^{\infty} d_m(n)\, p(t - nT) \tag{2.8}$$

and the transmitted signal vector is defined as

$$\mathbf{s}(t) = \begin{bmatrix} s_1(t) \\ s_2(t) \\ s_3(t) \\ \vdots \\ s_M(t) \end{bmatrix}. \tag{2.9}$$

2.2 Channel Model

The signal $s_m(t)$ is passed through a multiple-input multiple-output (MIMO) wireless channel. A MIMO channel with M users, each with a single transmitting antenna, and one receiver with L receive antennas is shown in Fig. 2.3. Let $h_{lm}(t)$ be the channel impulse response between the m^{th} user and the l^{th} receive antenna. The overall channel impulse response matrix is given by the $L \times M$ matrix $\mathbf{H}_{ct}(t)$ with

$$\mathbf{H}_{ct}(\tau,t) = \begin{bmatrix} h_{11}(\tau,t) & h_{12}(\tau,t) & \dots & h_{1M}(\tau,t) \\ h_{21}(\tau,t) & h_{22}(\tau,t) & \dots & h_{2M}(\tau,t) \\ \vdots & \vdots & \ddots & \vdots \\ h_{L1}(\tau,t) & h_{L2}(\tau,t) & \dots & h_{LM}(\tau,t) \end{bmatrix}, \tag{2.10}$$

where the subscript '*ct*' denotes the continuous time notation. The output of the channel is the convolution of the transmitted signal with the channel impulse response.

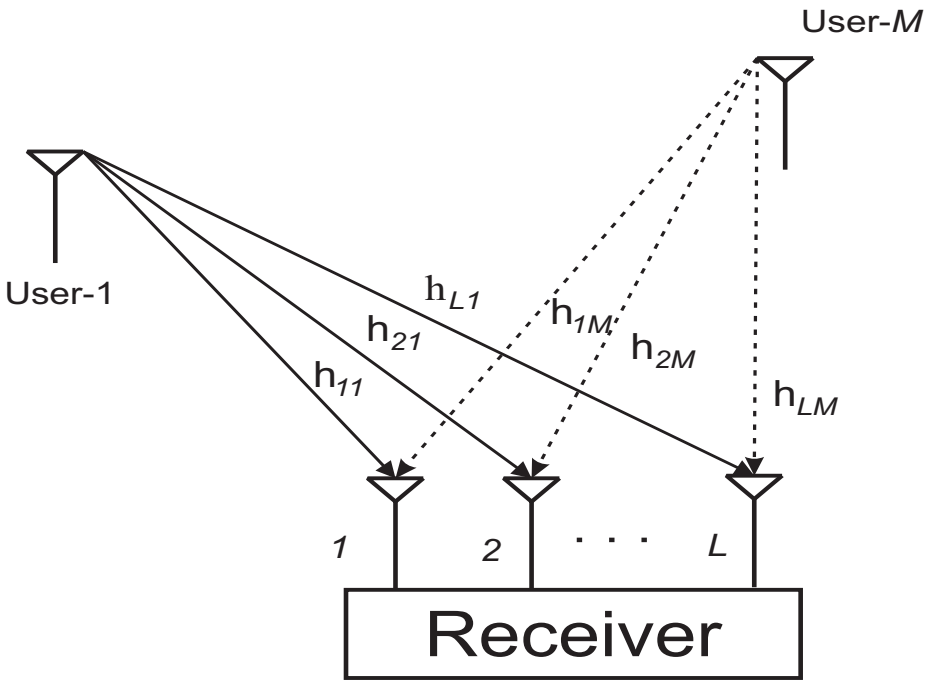

Figure 2.3: MIMO channel

2.3 Receiver

Multiuser receivers are mainly divided into two categories: the Optimal Maximum Likelihood Sequence Estimation (MLSE) receiver and the sub-optimal receivers [18, 19]. Since the complexity of an optimal receiver increases exponentially

with the length of channel time dispersion, they are computationally expensive to implement for most practical channels. An alternative to the optimal receiver is the minimal complex sub-optimal receiver. Two types of sub-optimal receivers are available, linear and non-linear sub-optimal receivers. A brief explanation of linear MMSE receivers is provided in this thesis.

A base station receiver with L antenna elements is considered as shown in Fig. 2.1. The signal received at the antenna element l is given by

$$r_l(t) = \sum_{m=1}^{M} h_{l,m}(\tau, t) \otimes s_m(t) + n_l(t). \tag{2.11}$$

This equation can be written in matrix form as given by

$$\mathbf{r}(t) = \mathbf{H}_{ct}(\tau, t) \otimes \mathbf{s}(t) + \mathbf{n}(t) \tag{2.12}$$

where $\mathbf{n}(t) = [n_1(t)\ n_2(t)\ n_3(t)\ \ldots\ n_l(t)]^T$ is the noise vector and $\otimes$ denotes the matrix convolution, and T denotes transpose.

The complex baseband signal $\mathbf{r}(t)$ from L antenna branches is applied to the MMSE linear combiner for joint detection of the users' data. A multiuser joint detection is used because of its significant performance improvement over single user detection [20] and the output of the linear combiner is sampled at the symbol rate before applying to the decision unit. In order to perform the adaptation in digital form, the sampler at the output of the linear combiner is moved to the input of the linear combiner. From Eq. 2.11 the received signal $r_l(t)$ can be written as

$$\begin{aligned} r_l(t) &= \sum_{m=1}^{M} h_{l,m}(\tau) \otimes \sum_{i=-\infty}^{\infty} s_m(i)\delta(t - iT) + n_l(t) \\ &= \sum_{m=1}^{M} \sum_{i=-\infty}^{\infty} s_m(i)\, h_{l,m}(t - iT) + n_l(t) \end{aligned} \tag{2.13}$$

where $s_m(i)$ is the sequence of data symbols that is transmitted by user m. Now this signal is sampled at the symbol rate to obtain a discrete time signal, which can be written as [21]

$$\begin{aligned} r_l(kT) &= \sum_{m=1}^{M} \sum_{i=-\infty}^{\infty} s_m(i)\, h_{l,m}(kT - iT) + n_l(kT) \\ &= \sum_{m=1}^{M} \sum_{i=-\infty}^{\infty} s_m(i)\, h_{l,m}((k-i)T) + n_l(kT) \end{aligned} \tag{2.14}$$

For notational simplicity, the T spaced signal sample received at the antenna element l can be written as

$$r_l(k) = \sum_{m=1}^{M} \sum_{i=0}^{n_c-1} s_m(i)\, h_{i,l,m}(k-i) + n_l(k), \tag{2.15}$$

where n_c is the number of channel coefficients, M is the number of users in the system and $h_{i,l,m}$ denotes the channel impulse response coefficient and $n_l(k)$ is the complex white Gaussian noise. The channel impulse response coefficient matrix $\mathbf{h}_{l,m}$ is defined as

$$\mathbf{h}_{l,m} = \begin{bmatrix} h_{0,l,m} & h_{1,l,m} & h_{2,l,m} & \dots & h_{n_c-1,l,m} \end{bmatrix}. \tag{2.16}$$

The channel impulse response convolution matrix $\mathbf{H}_{l,m}$ for the m^{th} user and the l^{th} receive antenna with dimensions $n_F \times (n_c + n_F - 1)$ is defined as

$$\mathbf{H}_{l,m} = \begin{bmatrix} h_{0,l,m} & h_{1,l,m} & \dots & h_{n_c-1,l,m} & 0 & 0 & \dots & 0 \\ 0 & h_{0,l,m} & h_{1,l,m} & \dots & h_{n_c-1,l,m} & \ddots & \ddots & 0 \\ 0 & 0 & h_{0,l,m} & h_{1,l,m} & \dots & h_{n_c-1,l,m} & \ddots & \vdots \\ \vdots & \ddots & \ddots & \ddots & \ddots & \ddots & \ddots & 0 \\ 0 & 0 & \dots & 0 & h_{0,l,m} & h_{1,l,m} & \dots & h_{n_c-1,l,m} \end{bmatrix}, \tag{2.17}$$

where n_F is the number of filter coefficients. Now the overall channel impulse response matrix $\mathbf{H}$ can be defined as

$$\mathbf{H} = \begin{bmatrix} \mathbf{H}_{1,1} & \mathbf{H}_{1,2} & \mathbf{H}_{1,3} & \dots & \mathbf{H}_{1,M} \\ \mathbf{H}_{2,1} & \mathbf{H}_{2,2} & \mathbf{H}_{2,3} & \dots & \mathbf{H}_{2,M} \\ \mathbf{H}_{3,1} & \mathbf{H}_{3,2} & \mathbf{H}_{3,3} & \dots & \mathbf{H}_{3,M} \\ \vdots & \vdots & \vdots & \dots & \vdots \\ \mathbf{H}_{L,1} & \mathbf{H}_{L,2} & \mathbf{H}_{L,3} & \dots & \mathbf{H}_{L,M} \end{bmatrix}. \tag{2.18}$$

and the received signal vector $\mathbf{r}(k)$ is defined as

$$\mathbf{r}(k) = \mathbf{H}\,\mathbf{s}(k) + \mathbf{n}(k). \tag{2.19}$$

The $M \times 1$ transmitted signal vector $\mathbf{s}(k)$ is defined as

$$\mathbf{s}(k) = \begin{bmatrix} \mathbf{s}_1(k) \\ \mathbf{s}_2(k) \\ \mathbf{s}_3(k) \\ \vdots \\ \mathbf{s}_M(k) \end{bmatrix}, \tag{2.20}$$

with

$$\mathbf{s}_m(k) = \left[\begin{array}{ccccc} s_m(k) & s_m(k-1) & s_m(k-2) & \dots & s_m(k-n_F-n_c+2) \end{array} \right]^T. \quad (2.21)$$

$\mathbf{n}(k)$ is a $L \times 1$ zero-mean complex Gaussian noise vector defined as

$$\mathbf{n}(k) = \left[\begin{array}{c} \mathbf{n}_1(k) \\ \mathbf{n}_2(k) \\ \mathbf{n}_3(k) \\ \vdots \\ \mathbf{n}_L(k) \end{array} \right], \quad (2.22)$$

with

$$\mathbf{n}_l(k) = \left[\begin{array}{ccccc} n_l(k) & n_l(k-1) & n_l(k-2) & \dots & n_l(k-n_F+1) \end{array} \right]^T. \quad (2.23)$$

$\mathbf{r}(k)$ is a $L \times 1$ received signal vector at the input branches of linear combiner defined as

$$\mathbf{r}(k) = \left[\begin{array}{c} \mathbf{r}_1(k) \\ \mathbf{r}_2(k) \\ \mathbf{r}_3(k) \\ \vdots \\ \mathbf{r}_L(k) \end{array} \right], \quad (2.24)$$

with

$$\mathbf{r}_l(k) = \left[\begin{array}{ccccc} r_l(k) & r_l(k-1) & r_l(k-2) & \dots & r_l(k-n_F+1) \end{array} \right]^T. \quad (2.25)$$

2.3.1 Linear Space Time Processing

Since the transmitted signal is passing through a wireless channel with time varying characteristics, it undergoes degradation and causes difficulty in retrieving the original transmitted data. This degradation is due to the thermal noise and the inter-symbol interference (ISI). In addition to ISI, a cross channel interference (CCI) is also present in the system due to M users interfering with each other. Equalization techniques can be used to overcome these degradations.

A linear combiner that suppresses both the CCI and ISI is used in this thesis. Since there are M users and L receiving antenna elements in the system, the linear combiner used here will have L inputs and M outputs. The m^{th} output of the linear combiner is given by

$$\hat{d}_m(k) = \sum_{l=1}^{L} \sum_{i=0}^{n_F-1} w_{i,l,m}^{*}\, r_l(k-i) \tag{2.26}$$

which can be written as

$$\begin{aligned} \hat{d}_m(k) &= \sum_{l=1}^{L} \mathbf{w}_{l,m}^{H}\, \mathbf{r}_l(k) \\ &= \mathbf{W}_m^{H}\, \mathbf{r}(k). \end{aligned} \tag{2.27}$$

A block diagram representation of the linear combiner is shown in Fig. 2.4 and its detailed structure is shown in Fig. 2.5. The filter coefficients vector $\mathbf{W}_m^H$ is given by

$$\mathbf{W}_m^H = \begin{bmatrix} \mathbf{w}_{1,m}(k) \\ \mathbf{w}_{2,m}(k) \\ \mathbf{w}_{3,m}(k) \\ \vdots \\ \mathbf{w}_{L,m}(k) \end{bmatrix}, \tag{2.28}$$

with

$$\mathbf{w}_{l,m}(k) = \begin{bmatrix} w_{0,l,m} & w_{1,l,m} & w_{2,l,m} & \dots & w_{n_F-1,l,m} \end{bmatrix}^T. \tag{2.29}$$

The error term is obtained by comparing the received signal $\hat{d}_m(k)$ with the transmitted sequence, and is defined as

$$e_m(k) = d_m[k] - \hat{d}_m(k) \tag{2.30}$$

The error term is used to update the weight vectors of the transversal filters in the linear combiner. The performance criterion used to update the weight vectors is the mean squared error (MSE) criterion given by

$$\epsilon = \mathbf{E}[|e_m(k)|^2]. \tag{2.31}$$

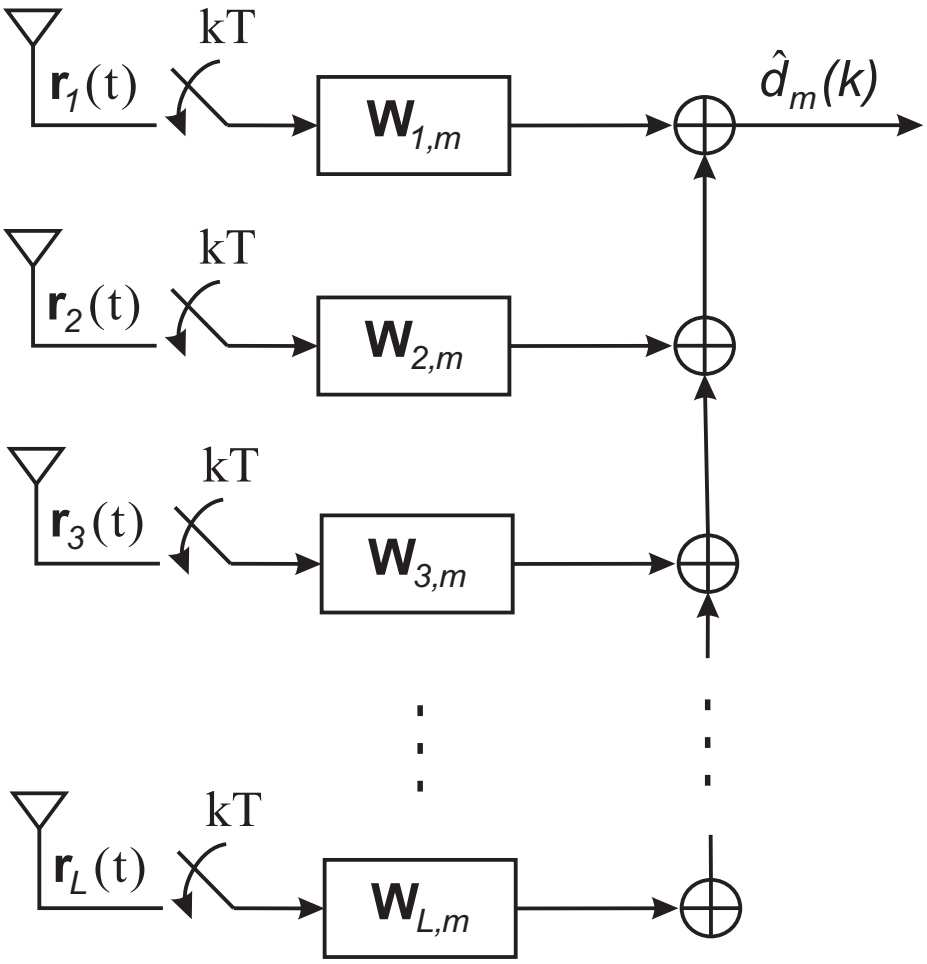

Figure 2.4: Block diagram of linear combiner for user m.

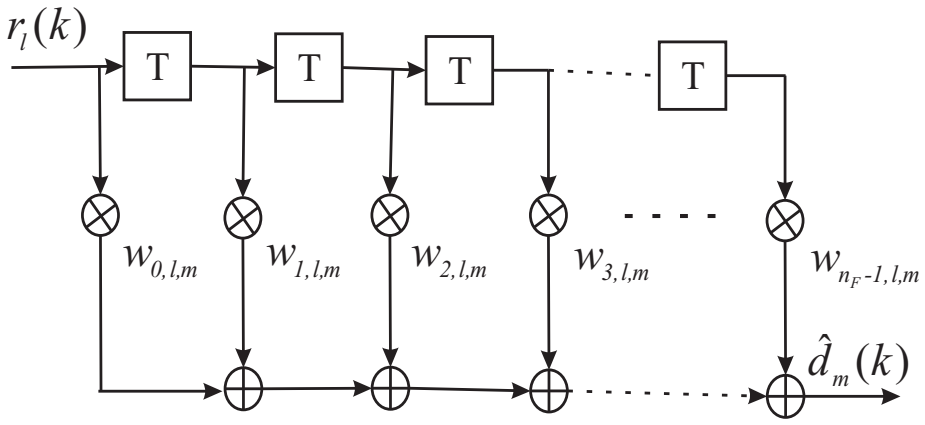

Figure 2.5: Detailed structure of the transversal filter.

Evaluating the above equation gives the term in the equation

$$\begin{aligned}
\epsilon &= \mathbf{E}[|e_m(k)|^2] \\
&= \mathbf{E}[(d_m[k] - \hat{d}_m(k))^2] \\
&= \mathbf{E}[(d_m - \mathbf{W}_m^H \mathbf{r})^2] \\
&= \mathbf{E}[(d_m - \mathbf{W}_m^H \mathbf{r})(d_m - \mathbf{W}_m^H \mathbf{r})] \\
&= \mathbf{E}[d_m^2 - d_m \mathbf{W}_m^H \mathbf{r} - \mathbf{W}_m^H \mathbf{r}\, d_m + \mathbf{W}_m^H \mathbf{r}\, \mathbf{W}_m^H \mathbf{r}] \\
&= \mathbf{E}[d_m^2 - d_m \mathbf{W}_m^H \mathbf{r} - \mathbf{W}_m^H \mathbf{r}\, d_m + \mathbf{W}_m^H \mathbf{r}\, \mathbf{W}_m \mathbf{r}^H] \\
&= \mathbf{E}[d_m^2 - 2\, d_m \mathbf{W}_m^H \mathbf{r} + \mathbf{W}_m^H \mathbf{r}\, \mathbf{r}^H \mathbf{W}_m] \\
&= \mathbf{E}[d_m^2] - 2\, \mathbf{W}_m^H \mathbf{E}[d_m \mathbf{r}] + \mathbf{W}_m^H \mathbf{E}[\mathbf{r}\, \mathbf{r}^H]\, \mathbf{W}_m \\
&= \sigma_d^2 - 2\, \mathbf{W}_m^H \mathbf{f} + \mathbf{W}_m^H \mathbf{R}\, \mathbf{W}_m \qquad (2.32)
\end{aligned}$$

where $\mathbf{f} = \mathbf{E}[d_l\, \mathbf{r}]$ is the cross correlation vector of d_l and $\mathbf{r}$, and $\mathbf{R} = \mathbf{E}[\mathbf{r}\, \mathbf{r}^H]$ is the autocorrelation matrix of $\mathbf{r}$. The MSE term is a function of filter tap coefficients and can be minimized by using three different methods. They are completing the squares, taking the gradient and statistical orthogonality. In this thesis a gradient method is used for minimizing the MSE. The procedure is to take the gradient

of the MSE with respect to the filter tap coefficients and equating that to zero to obtain a global minimum. This gives the final expression for optimum filter coefficients as given by

$$\mathbf{W}_{m_{opt}} = \mathbf{R}^{-1}\,\mathbf{f}. \tag{2.33}$$

This is called the Wiener solution. In order to find the optimum filter coefficients $\mathbf{W}_{m_{opt}}$ from 2.33, a set of linear equations have to be solved. Another way of obtaining the optimum filter coefficients without solving Eq. 2.33 explicitly is to use simple adaptive schemes such as steepest descent algorithm and the stochastic gradient algorithm, also called as the Least Mean Square (LMS) algorithm. An LMS algorithm is used in this thesis because of its simplicity. The LMS algorithm is basically a two-step process. First it computes the estimation error by comparing the filter's output response with the desired response. Second it updates the filter coefficients adaptively based on the estimation error. The optimal filter coefficient values obtained using the LMS algorithm are close to the Wiener solution values. The procedure for the LMS algorithm is to set the filter coefficients to some arbitrary values initially, and gradually move towards the optimum values by reducing the MSE value. At any time, the succeeding values of the filter coefficient vector are obtained according to the relation

$$\mathbf{W}_m(k+1) = \mathbf{W}_m(k) \;+\; \mu\, e_m(k)\, \mathbf{r}(k) \tag{2.34}$$

where $\mathbf{W}_m(k+1)$ is the updated value of tap weight vector, $\mathbf{W}_m(k)$ is the current value and μ is the adaptation coefficient, which is chosen to be sufficiently small. In order to update the filter coefficients, a training sequence is incorporated into the data sequence, and during this training the receiver knows the transmitted sequence and updates the filter coefficients to a global minimum based on MSE. This operation adapts the receiver to the variations in the channel and once the

training period is complete, the receiver switches to operate in normal mode. In order to converge to a minimum mean squared error, the training symbols required by an LMS algorithm are at least 10 times the number of filter coefficients to be updated [22].

The adaptation coefficient μ (or step size parameter) plays an important role in the convergence of the LMS algorithm. When μ is very small, the rate of convergence is slow, but the MSE obtained after adaptation is small. It also requires a large number of training symbols to adapt to a minimum MSE. On the other hand when μ is large, the rate of convergence is fast, but the MSE obtained after adaptation degrades when compared with small step size. So, the value of μ must be chosen in such a way that the convergence rate is not too slow or too fast. The main disadvantage of an LMS algorithm is its slow convergence rate.

2.3.2 Fractionally Spaced Equalizer

The detailed explanation given so far is for the symbol spaced equalizer, i.e., the received samples and the equalizer tap coefficients are spaced at the reciprocal of the symbol rate $1/T$. The T spaced equalizer performance is very sensitive to the sampling delay and channel delay distortion. It has been demonstrated that an equalizer can achieve higher performance, if the tap spacing of the equalizer is slightly smaller than T [23, 24, 25, 26]. Such an equalizer is called the Fractionally Spaced Equalizer (FSE) and it can effectively compensate for the channel delay distortion and sampling phase.

The main limitation of the T-spaced equalizer is due to the symbol rate sampling of the received signal at its input. This causes spectral overlap or aliasing and the overlapping components may add constructively or destructively based on the phases of the components. This results in the variation of the amplitudes in the frequency spectrum. In addition, the sampling phase variation results in

variable delay of the signals, which affects the amplitude and delay characteristics in the spectral overlap regions. Since the T spaced equalizer cannot compensate the received signal beyond the Nyquist frequency, the nulls created in the rolloff regions cannot be compensated properly.

In contrast, the FSE is based on sampling the received signal at higher than the symbol rate, so there will be no spectral overlap at the equalizer's input. In general a digitally implemented FSE has tap spacing of KT/N, where K and N are integers and $N > K$.

The mathematical analysis for the FSE is similar to the T spaced equalizer except that the input of the equalizer is sampled at higher symbol rates and the output of the equalizer is downsampled to the symbol rate. The filter coefficients are updated based on the LMS algorithm.

Chapter 3

UWB channel measurements

The performance of a wireless communication system is mainly limited by the propagation channel because of its random nature. Unlike wired channels, wireless channels are not stationary and predictable in nature. The propagation channel can be a simple line of sight (LOS) channel or a non line of sight (NLOS) channel that is severely obstructed by buildings, mountains and foliage in outdoor environments or by walls, furniture, and people in indoor environments.

Due to reflection, scattering, diffraction and refraction, the received signal consists of multiple distorted copies of the transmitted signal. This is called the multipath effect and it is the task of the receiver to mitigate these effects. A complete discussion of the channel propagation and channel modeling is beyond the scope of this thesis. There are many research papers and books dedicated for the radio propagation and channel modeling [27, 28, 29, 30].

This chapter is mainly divided into three parts, the first part provides a brief explanation of the antenna simulation and fabrication, the second part describes the different techniques to measure the radio channels and the final part provides a brief explanation of the experimental setups used to measure both the two-by-two and the three-by-three channels.

3.1 Antenna

Unlike narrowband, UWB antenna designers face a number of challenges because UWB antennas are required to attain a very wide impedance bandwidth and near omni-directional characteristics for the entire UWB spectrum. In addition, a linear phase characteristic is required for optimal pulse transmission and reception, because it reduces pulse distortion. Since UWB technology is mainly for portable electronic devices, commercially available UWB antennas (such as biconical and horn antennas) cannot be embedded in portable electronic devices and integrated circuits because of their size and cost.

Recent research work has been focused on designing planar, omni-directional antennas. A number of planar UWB antennas have been described in the literature [31]. Based on the antenna parameters such as impedance bandwidth, radiation pattern, directivity, efficiency and gain, a single ended elliptical antenna and a circular disc monopole antenna [32, 33] were selected. Finally a printed circular disc monopole antenna was simulated and fabricated as specified by Liang et al. [33]. The antenna simulations were performed using CST Microwave Studio and fabricated on an FR-4 substrate whose dielectric constant was 4.2. The length and width of the designed antenna were 50 mm and 42 mm respectively. A picture of the fabricated antenna is shown in Fig. 3.1.

Impedance bandwidth is an important parameter, which indicates the amount of power reflecting back from the antenna feed point due to impedance mismatch. The typical desired value of the return loss to indicate a good impedance match should be greater than or equal to 10 dB. This corresponds to a Voltage Standing Wave Ratio (VSWR) of 2:1. The return loss and the VSWR of the fabricated antennas were measured using an HP 8510B Vector Network Analyzer (VNA). The measured and simulated curves are shown in Fig. 3.2. It is clear from Fig. 3.2 that the measured results from the designed antenna have a VSWR

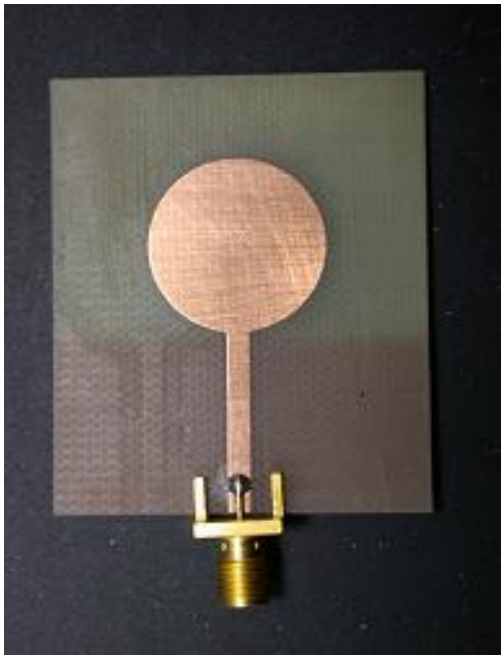

Figure 3.1: Picture of the fabricated antenna

of 2.2:1 or better in the $3.1 - 10$ GHz band and is close to the simulated value. The slight variations from the simulated values are most likely due to inadequate modelling of the coaxial to microstrip transition. The radiation pattern for this antenna is omni-directional [33].

3.2 UWB Channel Sounding

In order to obtain channel impulse responses, several channel sounding techniques have been presented in the literature [27, 34]. They are mainly classified as time domain or frequency domain channel sounding techniques.

3.2.1 Time-domain Channel Sounding

Time domain channel sounding technique uses short duration pulses to excite the channel and the received signal is captured and displayed on a high speed sampling oscilloscope. The main advantages of this technique are less complexity,

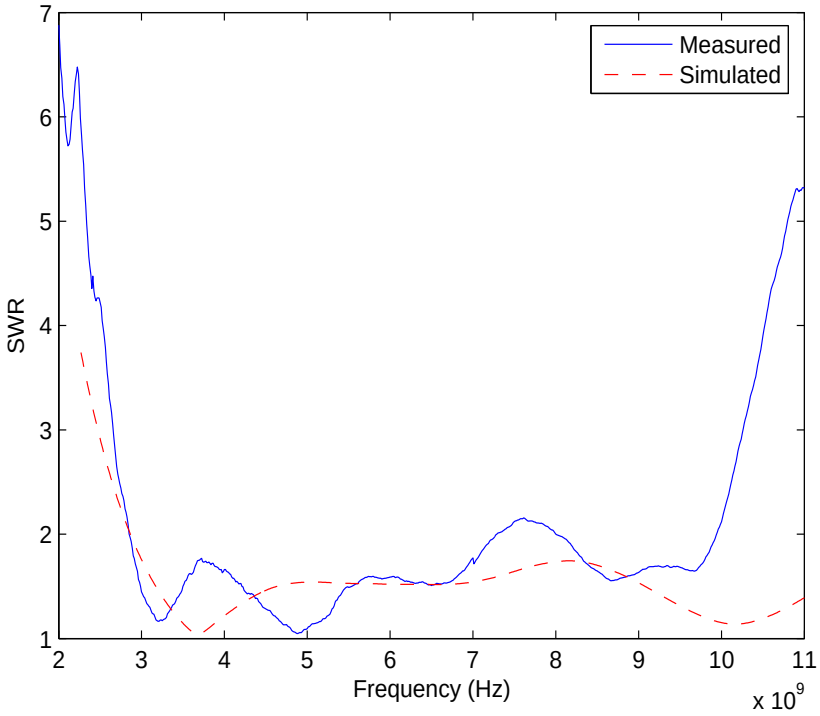

Figure 3.2: Comparison of measured and simulated VSWR

lower cost and the channel impulse responses are readily available in time domain. The main problem with this technique is that it requires the generation of very short duration pulses and is affected by the use of non-ideal transmit pulses, distorting the obtained channel impulse responses.

3.2.2 Frequency-domain Channel Sounding

The time and frequency domain techniques can be related using the Fourier transform, so, it is possible to obtain the channel impulse response from the frequency domain characteristics. The frequency domain channel impulse response measurement system is shown in the Fig. 3.3. The transmitter and receiver antennas are connected to the two test ports of the VNA. The VNA controls the synthesized frequency sweeper to sweep through the specified frequency band by stepping through discrete frequencies. An S-parameter test set is used to monitor the

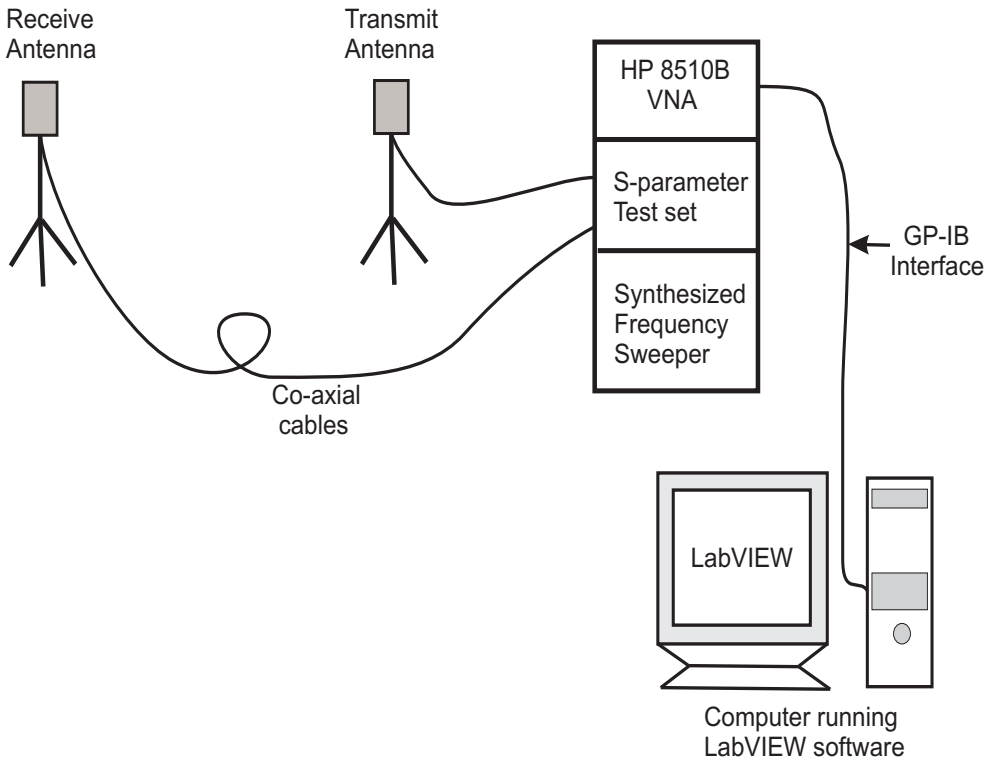

Figure 3.3: Frequency domain channel sounder measurement system

frequency response of the channel for every frequency step.

The channel's complex frequency response data from the HP 8510B VNA is collected using a computer running LabVIEW® software which is connected using a GP-IB interface. The time domain impulse responses are obtained by taking the inverse Fourier transform of the complex frequency responses and the MATLAB® code is given in Appendix A.1. A typical UWB LOS channel's frequency response and its corresponding time domain channel impulse response are shown in Figs. 3.4 and 3.5.

The main advantage of this technique is that the system has the calibration facility, which can calibrate for all the losses caused by cables and connectors. The main limitation is that longer cables are required to obtain channel impulse responses, because the transmit and receive ports are connected to the same device. So, this technique is mainly useful for close indoor measurements only. Another limitation is that it cannot record the variations of the time varying channels, but

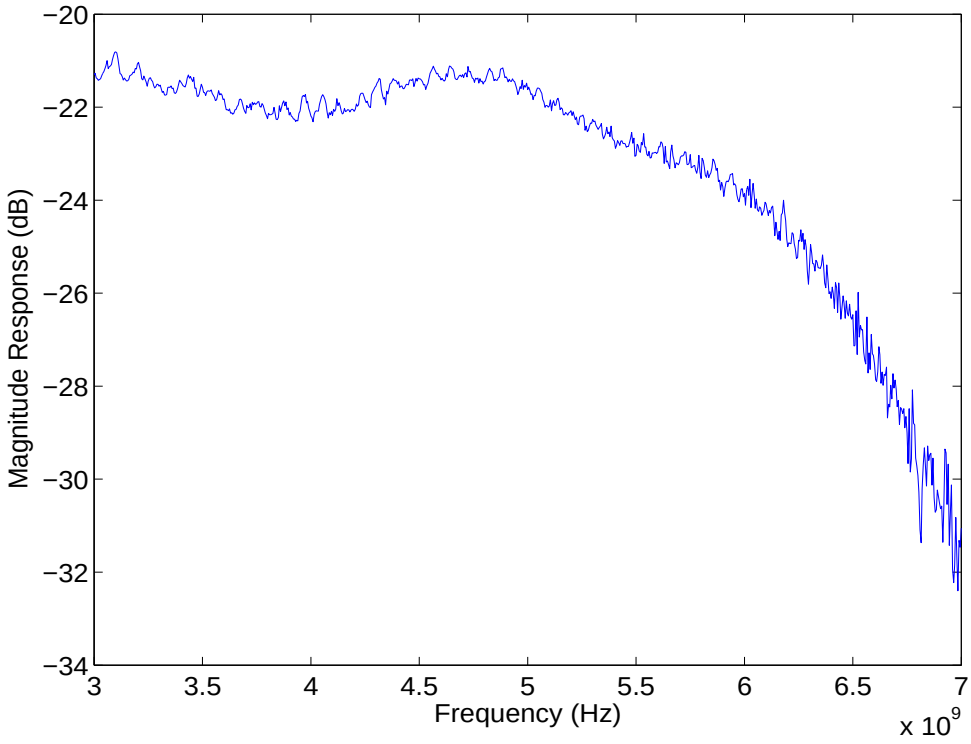

Figure 3.4: Typical UWB LOS frequency response of a channel.

this can be mitigated by employing faster sweep times.

3.3 Experimental Setup

3.3.1 Equipment

The equipment used for both the two-by-two and the three-by-three model channel measurements are five wooden stands of height 1.2 m, two slotted wooden supports of lengths 120 cm and 85 cm which are used for positioning the receiver antenna elements, two coaxial cables each of length 5 m and the remaining equipment was mentioned in the Sec. 3.2.2. The experimental setup for the channel measurement is shown in the Fig. 3.6.

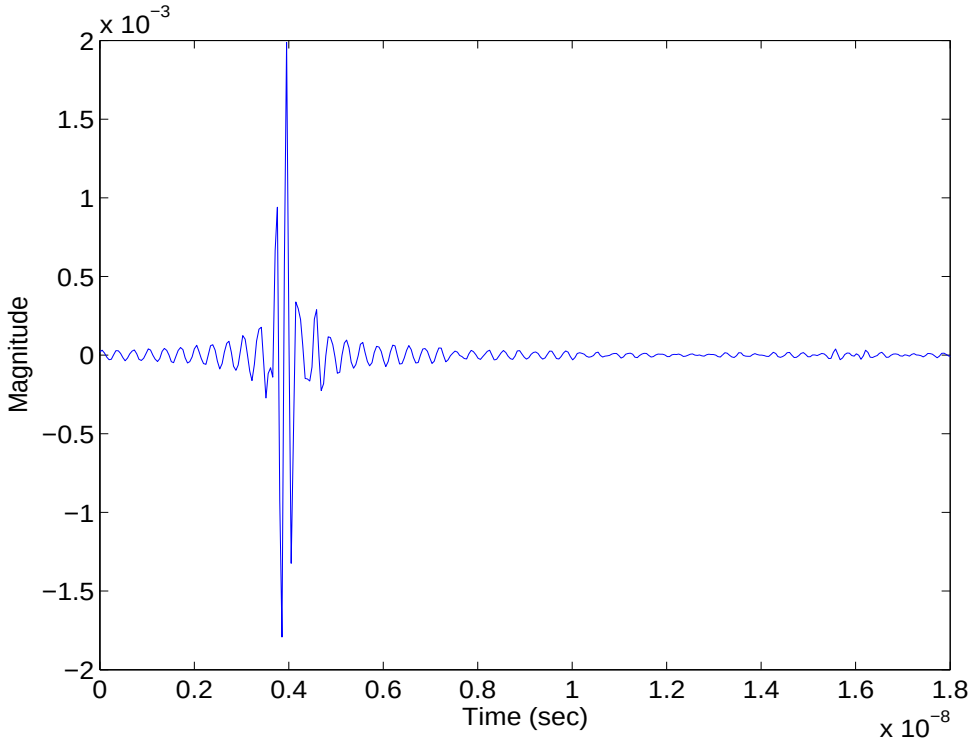

Figure 3.5: Typical UWB LOS impulse response of a channel.

3.3.2 Procedure

A frequency-domain technique is used to measure the UWB channel responses. In UWB the transmitter and receiver separation distance is mainly limited by the cables that connect them, because the high frequency components attenuate more quickly as the length increases. So, we used the vector network analyzer to sweep only from 3 GHz to 7 GHz using 801 points with a frequency step of 5 MHz. These measurements were performed in an anechoic chamber to emulate the MIMO LOS channels. The procedure for separating the antennas are shown in Figs. 3.7 and 3.8.

In both the two-by-two and the three-by-three cases, the transmit (Tx) and receive (Rx) antennas are in an LOS scenario and kept at a height of 120 cm from the floor. The antenna elements at the receiver are separated on the scale of a symbol-wavelength and the transmitters are placed randomly in a circle of

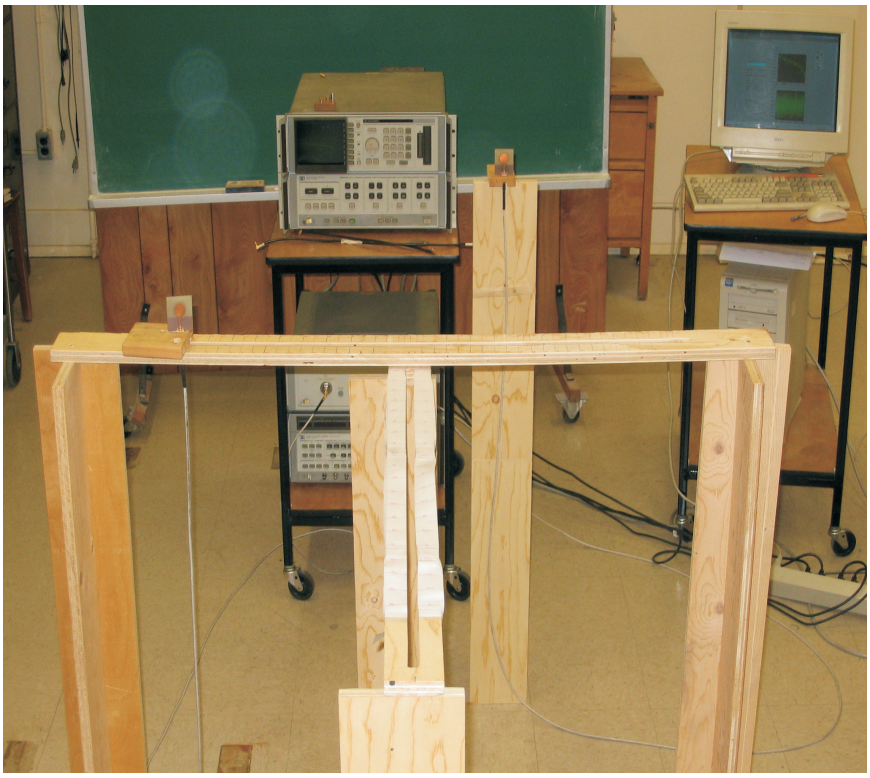

Figure 3.6: Experimental setup for the two-by-two and the three-by-three channel measurement case.

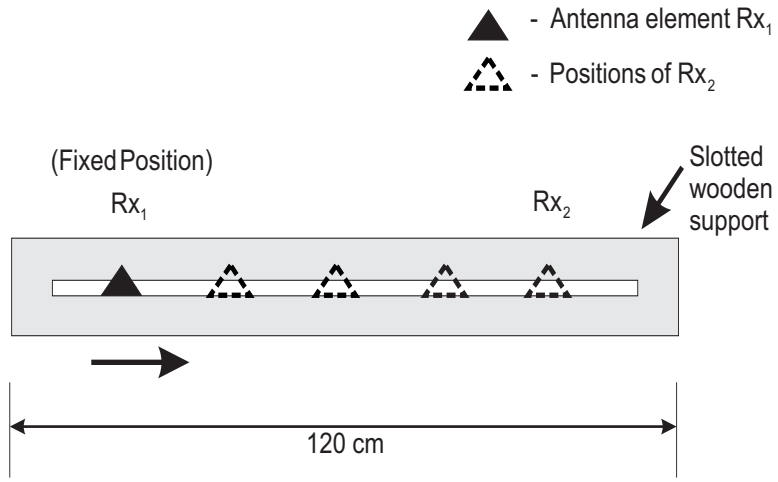

Figure 3.7: Receiver antenna positions setup (Top view) for the two-by-two channel measurement case.

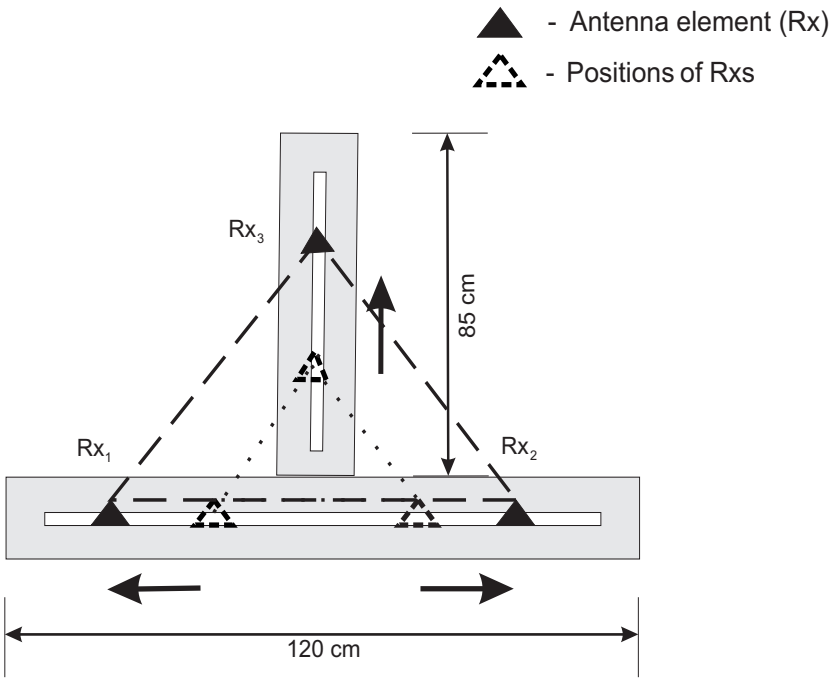

Figure 3.8: Receiver antenna positions setup (Top view) for the three-by-three channel measurement case.

radius 1 m. In a two-by-two case, the receiver antenna-element separations are varied from 2 cm to 4 cm in steps of 2 cm and from 4 cm to 80 cm in steps of 4 cm and in a three-by-three case, they are varied from 4 cm to 80 cm in steps of 4 cm. The arrows in Figs. 3.7 and 3.8 indicate the direction in which the antenna elements are moved.

In order to verify pathological case 1, i.e. when the transmitters are in even symmetry with respect to the receiver antenna elements, of Fig. 1.3(b), the transmitters are placed at a 45 degree angle from the receiver array axis on either side at a distance of 1 m from the midpoint of the 120 cm slotted wooden support. To verify the second pathological case, i.e. when the receiving antenna elements are in even symmetry with respect to the transmitters, the transmitters are placed at a 90 degree angle from the receiver array axis at distances of 1 m and 0.6 m[1].

In order to show that these pathological cases can be avoided by using a

[1]These distances can be varied as long as the receiving antenna elements are in angle symmetry with respect to transmitters.

three-by-three model, the two transmitters are placed in the locations mentioned above and the third transmitter is located randomly in a circle of radius 1 m, whose center is the midpoint of the 120 cm slotted wooden support. At each separation[2] nine radio channels are measured.

[2]The term separation refers to receiver antenna-element separation, unless otherwise stated.

Chapter 4

Simulation Results

This chapter describes the MATLAB® baseband simulation which is used to evaluate the MMSE performance in an uplink scenario for both the two-by-two and the three-by-three system models. Finally the simulation results for different antenna configurations are discussed.

4.1 Simulation Structure

The simulation used to implement the MIMO multiuser UWB system was based on the system model shown in Fig. 2.1. The simulation flowchart is shown in the Fig. 4.1. The passband to baseband routine converts the time-domain passband impulse responses to baseband impulse responses. At the beginning of the simulation, all the global parameters such as sampling frequency, symbol rate, operating frequency band, noise variance, number of users and number of antennas are initiated by the global routine. Randomly generated users' data is modulated using QAM modulation to obtain symbols. These symbols are pulse shaped using a root raised cosine filter before being transmitted into the wireless channel. At this instant, the measured baseband channel impulse responses are loaded into the simulation to emulate the MIMO channels. An AWGN is added to the received

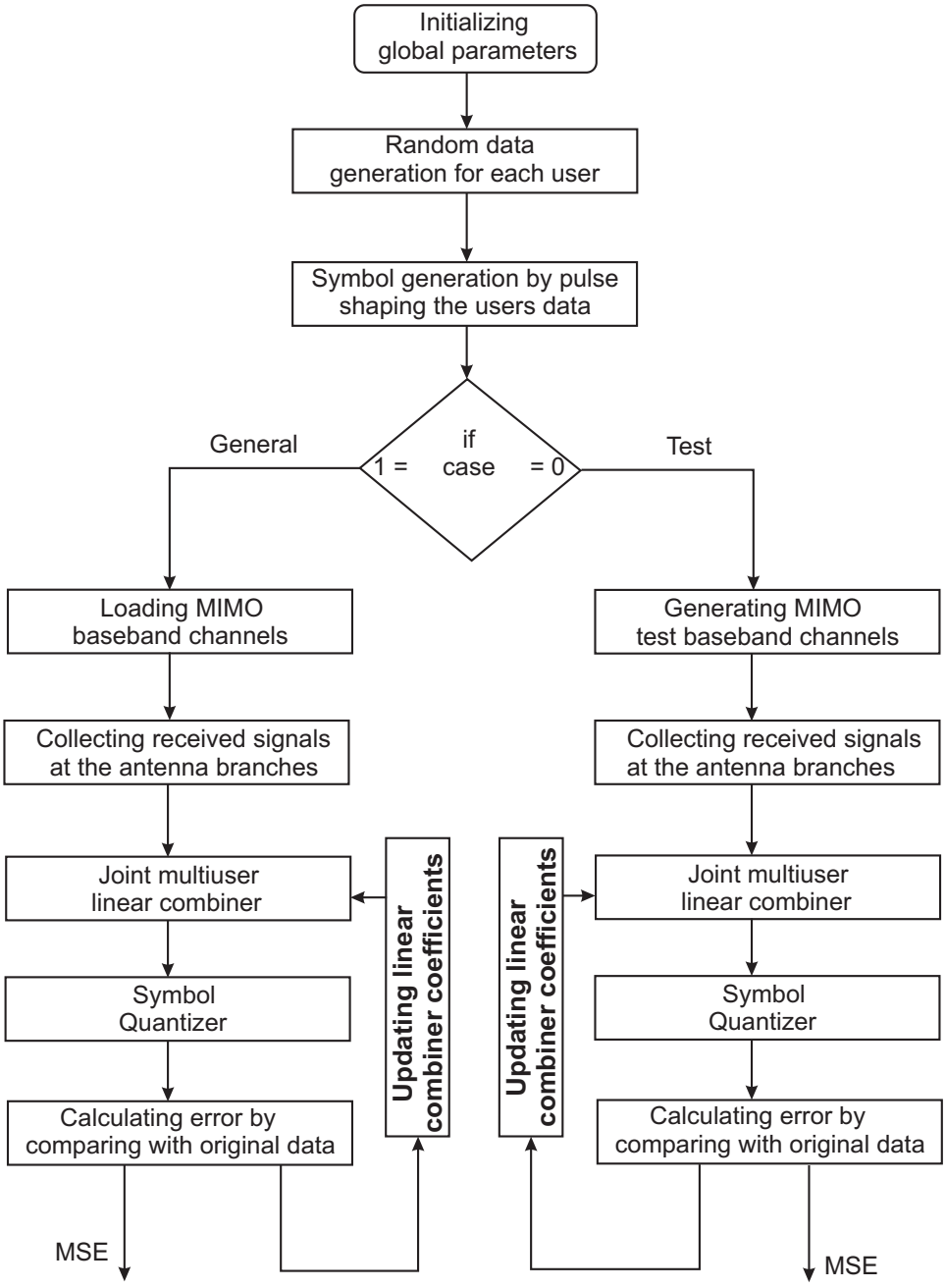

Figure 4.1: Flowchart structure of the MATLAB® simulation.

signals at the antenna branches. These signals are further processed using a linear combiner which cancels out the multiple access interference. A LMS algorithm was used to adapt the random variations of the signals caused by the wireless channels. Finally the MSE is calculated by comparing the received data with the original transmitted data.

In order to validate the developed simulation, a test simulation was also developed. The assumptions that were considered while developing the MATLAB® simulation are given below

- There is no coordination between users (i.e. each user's data is assumed to be independent),
- No error control mechanism was considered, but the simulation can be extended easily to implement this technique,
- The modulation scheme considered is 4-QAM, but the modulation scheme can be changed easily in the simulation,
- The number of antenna elements L employed at the receiver is equal to the number of users M in this simulation,
- A long training sequence of 2^{17} symbols and a step size of 0.002 was employed, to ensure the proper convergence of the LMS algorithm.

The learning curves for the LMS algorithm and the adapted linear combiner coefficients of the two-by-two system with different antenna separations from 2 cm to 4 cm are shown in the Figs. 4.2 and 4.3. From the figures it is clear that as the separation increases the value of the overall MSE decreases. A similar trend is followed for the three-by-three case as shown in the Figs. 4.4 and 4.7.

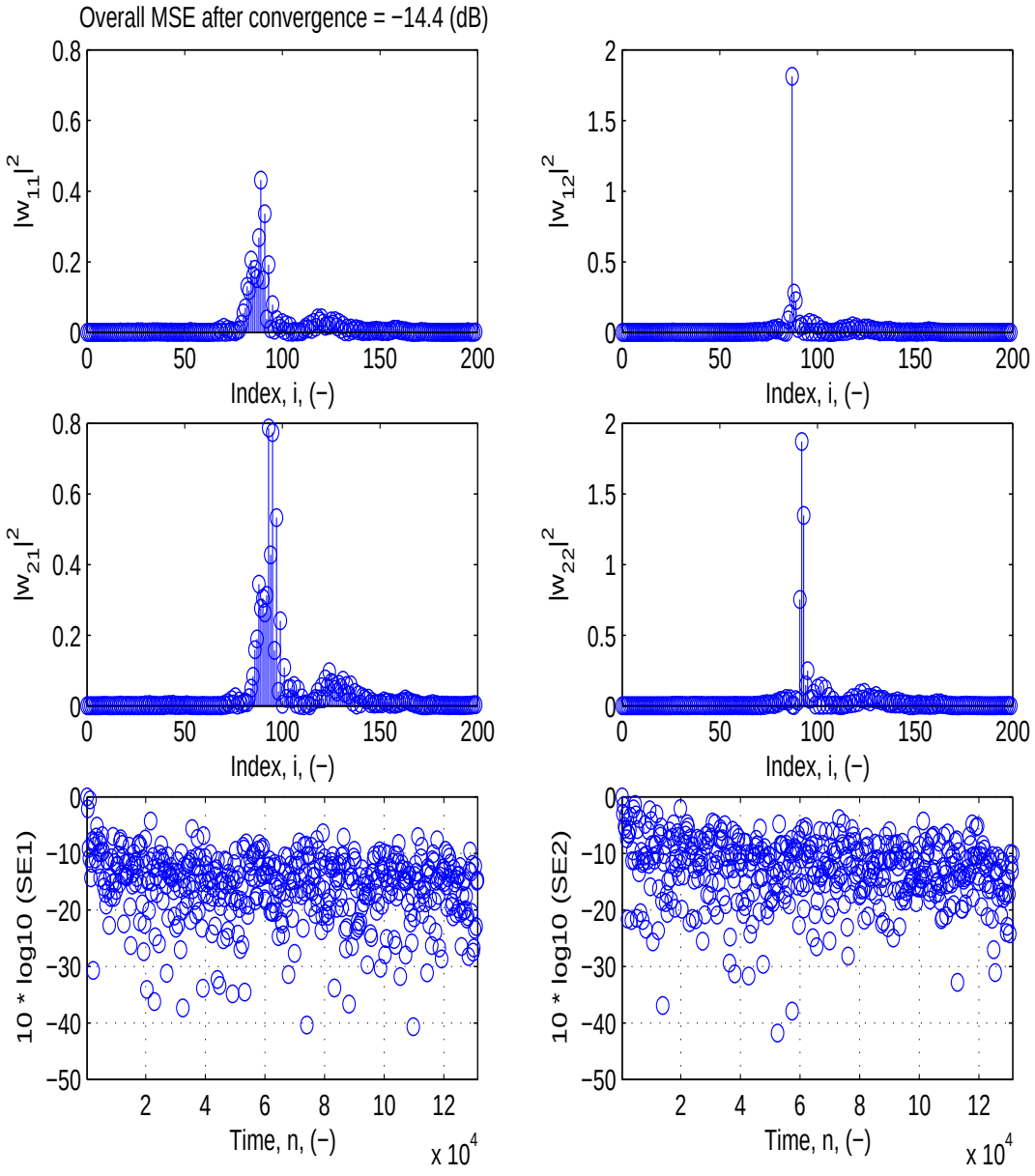

Figure 4.2: Linear combiner filter coefficients and the MSE learning curves plot for 2 cm separation in a two-by-two system.

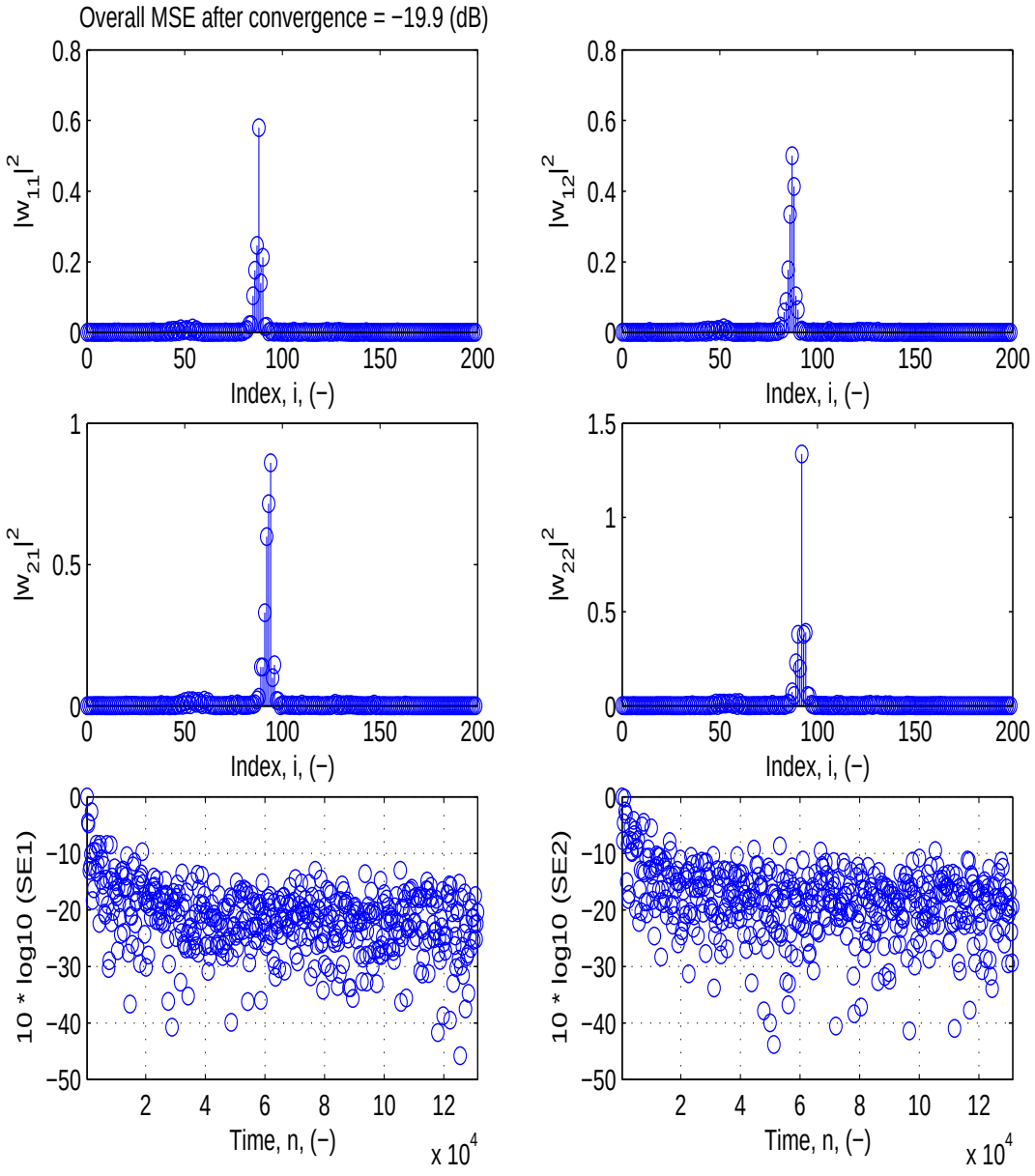

Figure 4.3: Linear combiner filter coefficients and the MSE learning curves plot for 4 cm separation in a two-by-two system.

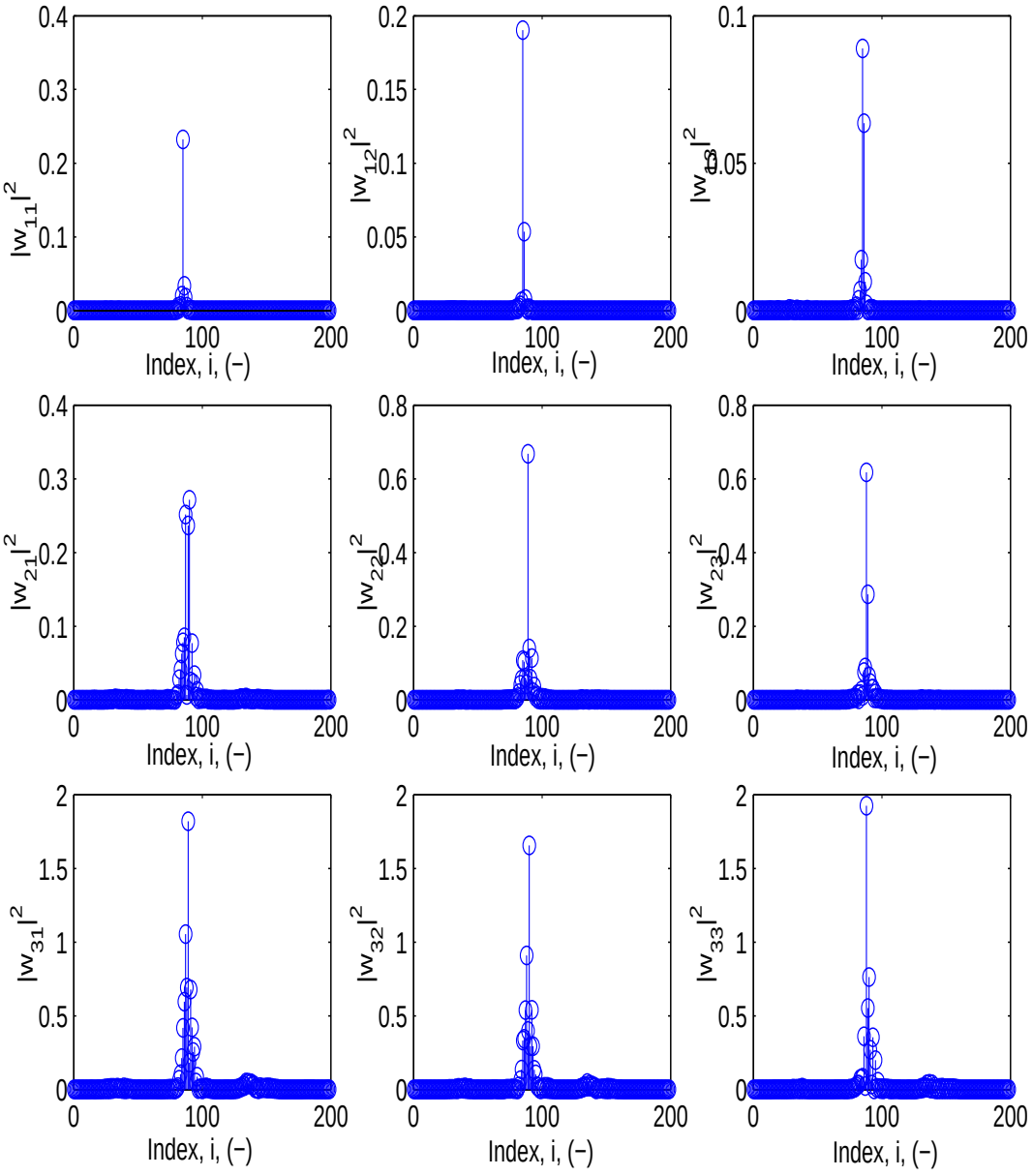

Figure 4.4: Linear combiner filter coefficients for 4 cm separation in a three-by-three system.

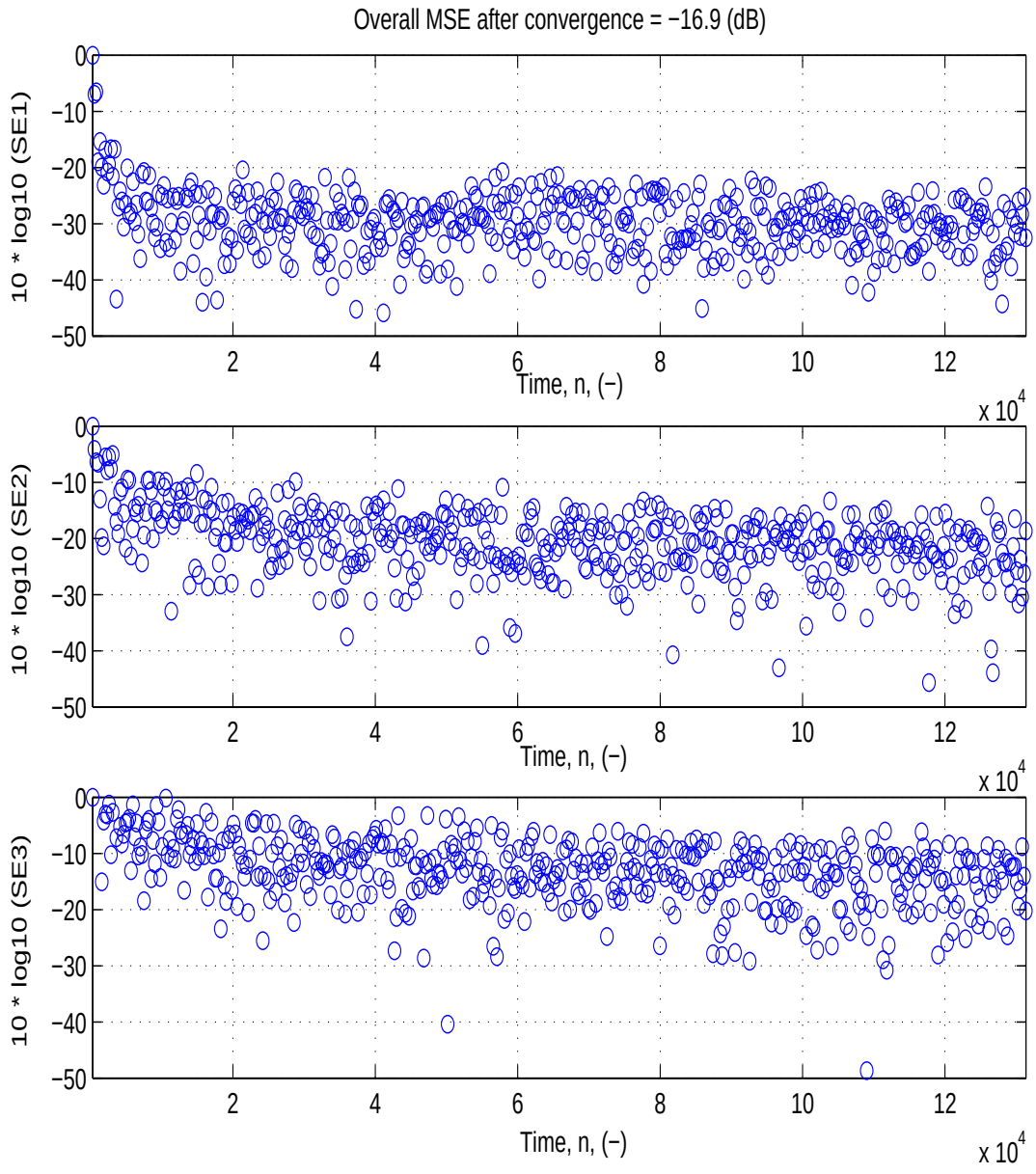

Figure 4.5: MSE learning curves for 4 cm separation in a three-by-three system

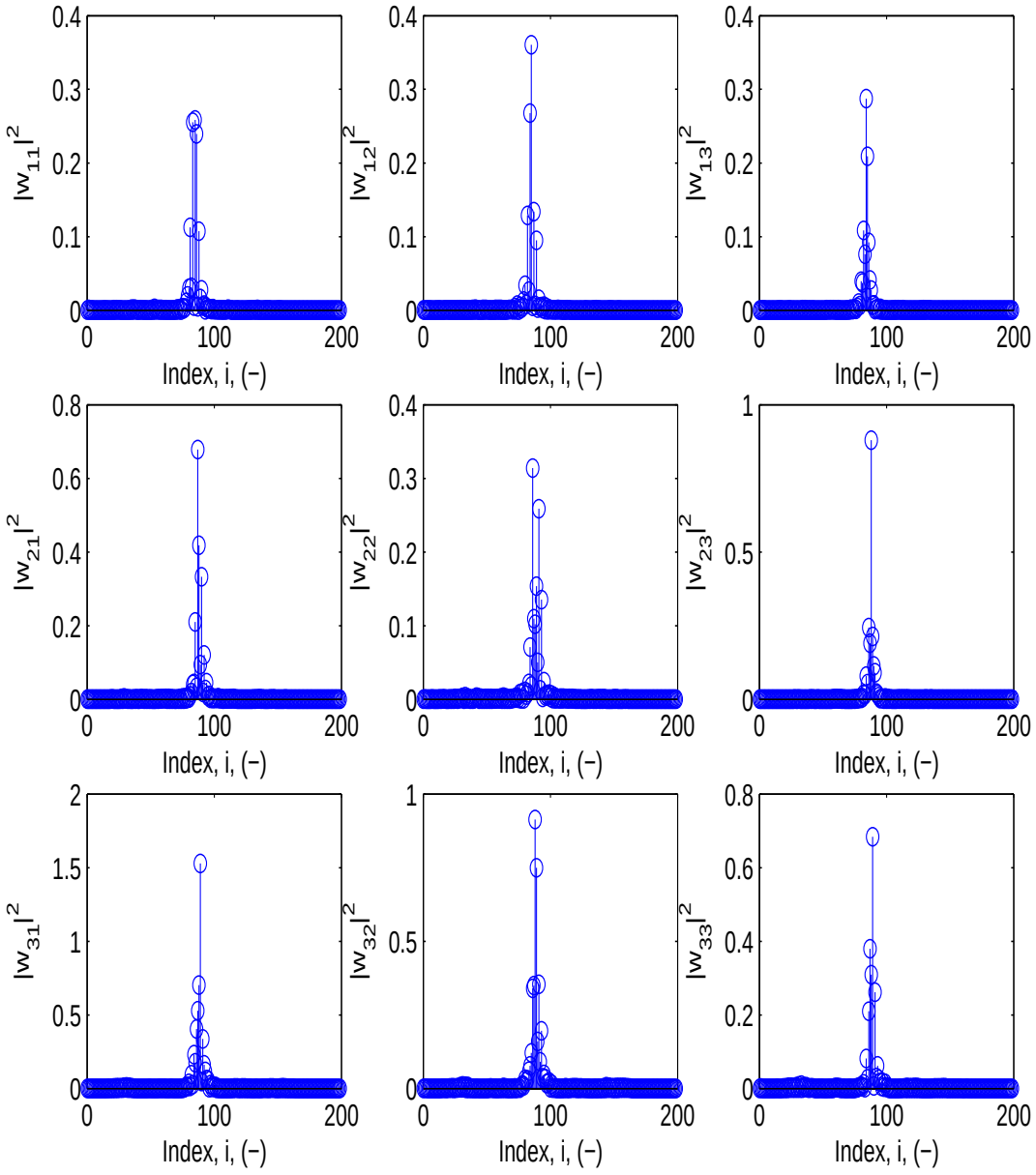

Figure 4.6: Linear combiner filter coefficients for 8 cm separation in a three-by-three system.

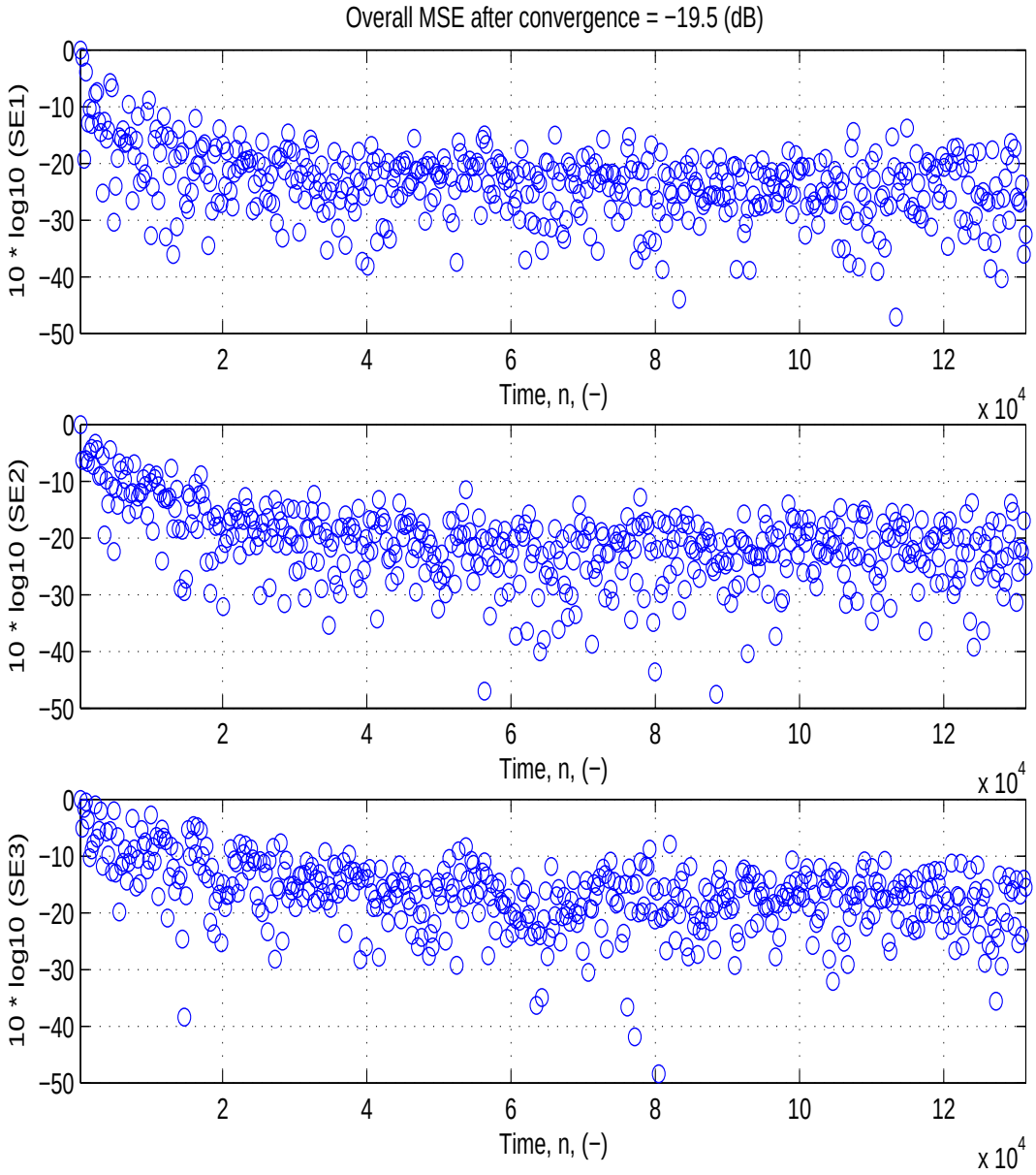

Figure 4.7: MSE learning curves for 8 cm separation in a three-by-three system.

4.2 Pathological Case Analysis

The results related to pathological cases are explained in this section. Figs. 4.8 and 4.9 show the two-by-two and three-by-three case MSE comparison when the transmitters are placed in pathological case 1 and case 2, respectively. It is clear from Fig. 4.8 that the three-by-three case MSE values are lower than the two-by-two case by a significant amount, over 4 dB.

As mentioned in the procedure for the two-by-two case, receiving antenna-element-1 (Rx_1) is fixed and the receiving antenna-element-2 (Rx_2) is moved away from Rx_1; until the separation reaches 76 cm, the transmitters are not in the pathological case. It is observed from Fig. 4.9 that until the separation reaches $4\lambda_T$, the MSE value is low. When the separation distance exceeds $4\lambda_T$, the MSE value increases. This is verified by observing the reduced delay between the received impulse responses as the separation distance was increased. In the three-by-three case, the MSE curve is almost constant when the separation distance approaches $3\lambda_T$. Pathological cases are very sensitive to the transmitter and receiver antenna-element positions; even a change of 0.5 cm can move the transmitters out of the pathological cases.

Figs. 4.10 and 4.11 show the MSE versus signal-to-noise ratio (SNR) comparison of pathological cases for the two-by-two and three-by-three systems. The baseband SNR before receiver is defined as the ratio of energy per symbol to the complex noise power spectral density. This is varied by changing the noise variance in the simulation. In order to show the SNR performance gain of a three-by-three system over a two-by-two system, we considered the case when the transmitters are in the pathological cases and varied the SNR. From the figures it is clear that as the value of SNR increases the MSE performance improves logarithmically for a three-by-three system in both of the pathological cases, but for a two-by-two system the performance improves until the SNR is 30 dB, following which there is

little improvement. At an SNR of 30 dB, if we convert the MSE values of two-by-two and three-by-three cases into dB, we observe 14.4 dB and 6.1 dB diversity gain for a three-by-three system in the pathological cases. From our measurements, in almost all of the cases, the three-by-three system outperforms the two-by-two system, as would be expected.

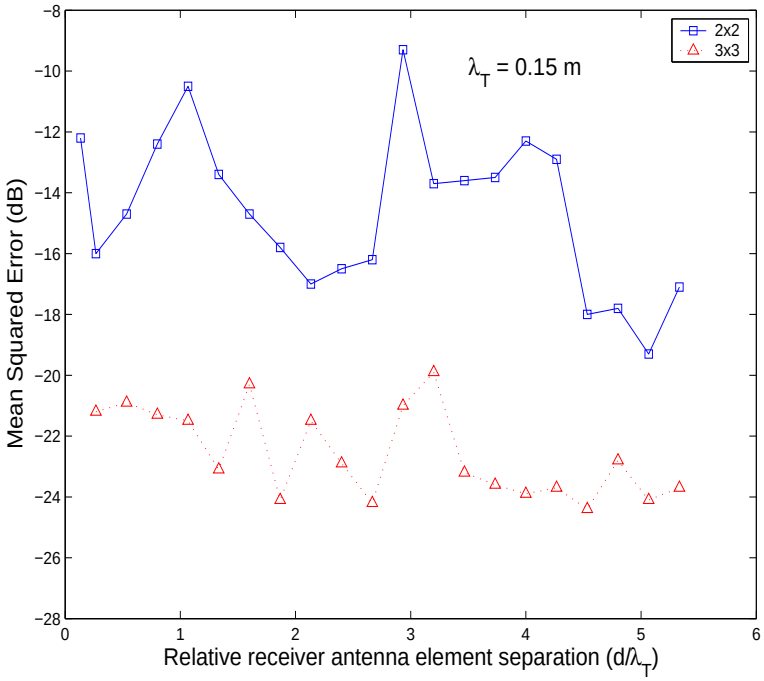

Figure 4.8: MSE comparison for the two-by-two and three-by-three pathological case 1.

4.3 Performance Comparison of the Two-By-Two and the Three-By-Three Systems

The MSE results of the two-by-two and the three-by-three models obtained through the simulation are analyzed in this section. Figs. 4.12 and 4.13 show the MSE for the measurement data of the two-by-two and three-by-three cases for random transmitter locations. Each vertical line in the two-by-two case corresponds to four data points, whereas in the three-by-three case it corresponds to five data

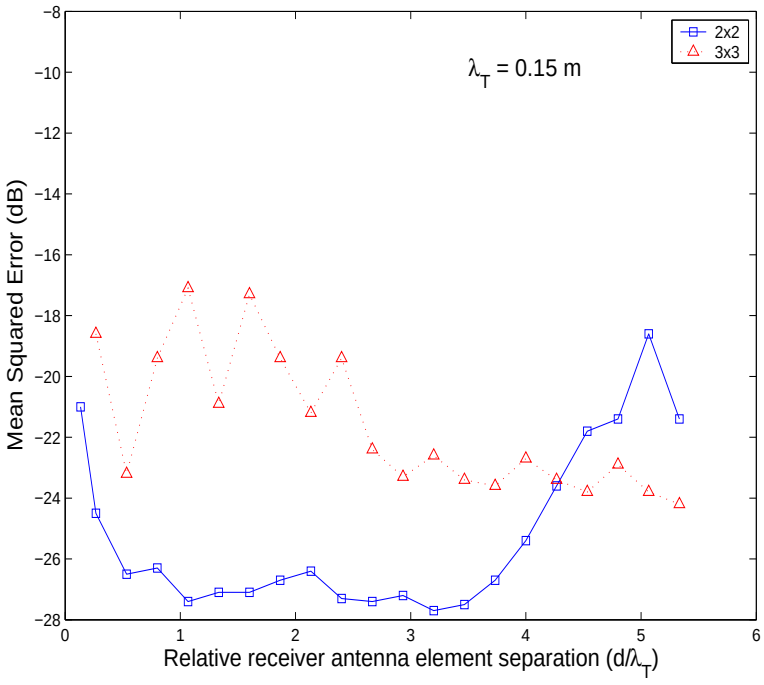

Figure 4.9: MSE comparison for the two-by-two and three-by-three pathological case 2.

points. It is clear from Fig. 4.12, that even though the mean value curve looks smooth, the actual values are more scattered until the separation distance approaches $4\lambda_T$. Further separation shows that the values are packed together with reduced variation. The standard deviation (σ) of each vertical line is calculated for each separation distance and the mean value of σ is found to be 4.97 dB. For the three-by-three case, the MSE values appear less scattered around the mean value and from the measured data, the value of σ is found to be 1.68 dB which is 3.3 dB less than the two-by-two case. From Fig. 4.13, it is also evident that when the antenna elements are separated by $3\lambda_T$ (45 cm) or more, there is no significant improvement in MSE values; they are almost constant[1].

It is also observed that the minimum attainable MMSE value in the two-by-two case is small when compared to the three-by-three case. This is due to the effect of increased interference in the system with an additional transmitter.

[1]As we are operating in such a wideband we expect a noise level of around -60 dBm to -50 dBm from outside sources and also thermal noise in the cables.

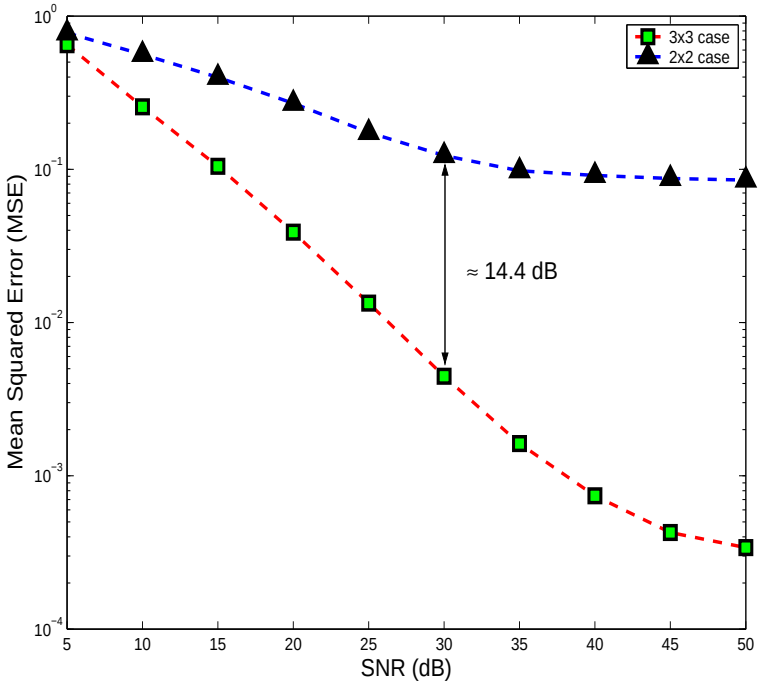

Figure 4.10: MSE vs SNR comparison for the two-by-two and three-by-three pathological case 1.

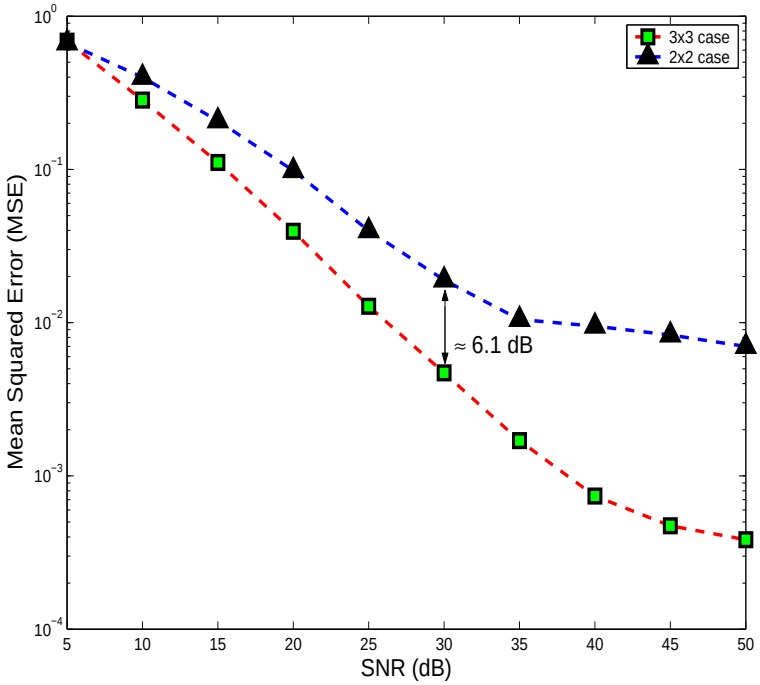

Figure 4.11: MSE vs SNR comparison for the two-by-two and three-by-three pathological case 2.

As the number of transmitters in the system increase, the amount of inter-user interference also increases.

Observations from the graphs reveal that an optimum receiver antenna-element separation of more than $4\lambda_T$ (60 cm) is required for a two-by-two system model and $3\lambda_T$ (45 cm) for a three-by-three system model. Lee proposed a triangular array configuration to separate antennas regardless of direction of arrival and specified that the separation can be reduced when a triangular array is used instead of a two element linear array [35]. Lee also showed that antenna-element separation of greater than 20 carrier wavelengths is required for smaller beamwidths in LOS channels for the broadside propagation case and an even greater separation distance of 70 carrier wavelengths is required for the in-line propagation case [36]. From the results it is clear that a receiver antenna-element separation of three symbol wavelengths is sufficient for a three-by-three model and more than four symbol wavelengths is required for a two-by-two model.

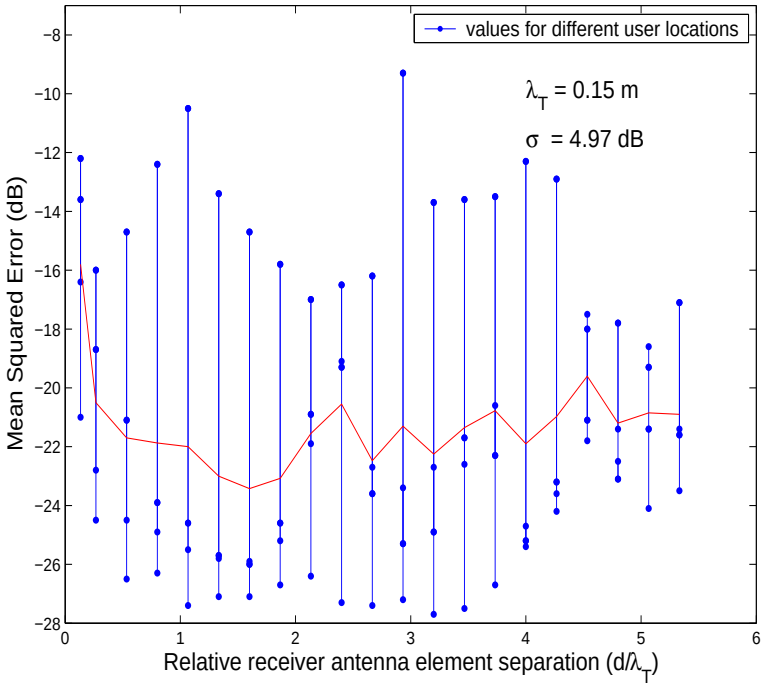

Figure 4.12: MSE vs relative receiver antenna element separation (d/λ_T) for the two-by-two case.

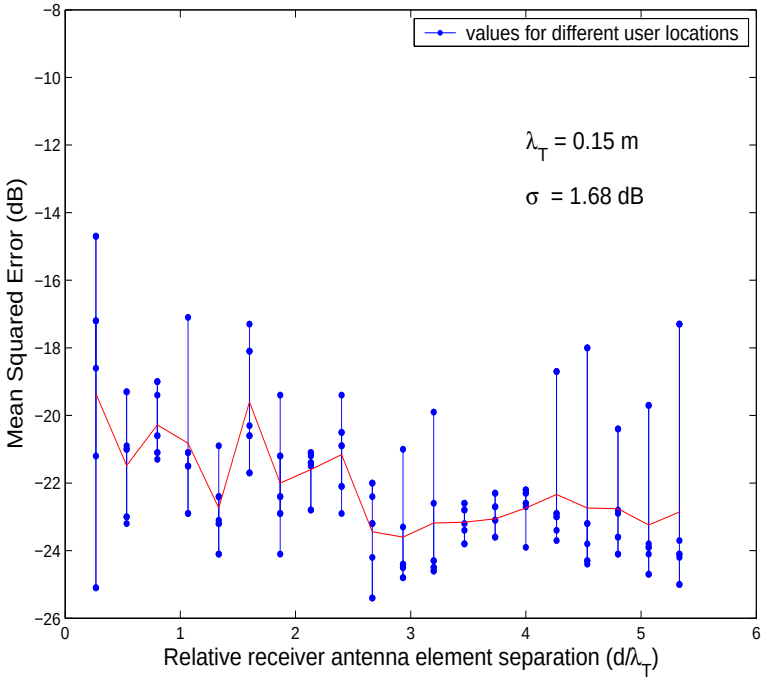

Figure 4.13: MSE vs relative receiver antenna element separation (d/λ_T) for the three-by-three case.

Chapter 5

Conclusion and Future work

5.1 Conclusion

An overview of a UWB MIMO multiuser system was presented in this thesis. The receiver antenna element separation in a near LOS channel was optimized based on a new parameter called symbol wavelength. A baseband simulation was developed to demonstrate the system performance for different antenna configurations. UWB LOS channel measurements were performed for both the two-by-two and three-by-three system models to incorporate in the simulation. The existence of pathological cases was verified in a two-by-two model and a three-by-three model with a triangular array configuration for the receiver was proposed to remove those pathological cases.

Simulation results show that the optimum receiver antenna-element separation is $3\lambda_T$ in a three-by-three case and more than $4\lambda_T$ in the two-by-two case. It was also observed that a diversity gain of 14 dB in pathological case 1 and 6 dB in pathological case 2, is achieved by using a triangular array in the three-by-three model.

5.2 Future work

In this thesis, the receiver antenna separation is quantified for the near LOS channels. This work can be extended to dense multipath channels to observe the effect of symbol wavelength. A more complex and faster adaptation algorithm can be employed instead of a simple LMS algorithm. Since measuring the channels is a time consuming process, it would be better to develop a channel model for both the near LOS channels and the dense multipath channels. A bandwidth of 7 GHz is available for the UWB applications, but only 4 GHz of bandwidth was used in this thesis due to lossy coaxial cables. This work can be extended to the complete 7 GHz bandwidth.

As the research work in the MIMO transceiver design for UWB is in the initial stage, designing and implementing a UWB MIMO transceiver on FPGA will be another future direction. As far as I know, no research paper has been available in the literature relating to the implementation of UWB MIMO transceivers on FPGA. Since the UWB applications require very high data speeds several design issues, such as the requirement of the high speed sampling ADCs and DACs have to be considered.

Bibliography

[1] H. Agus, "Ultra-wideband channel characterization and receiver analysis," M.Sc.E. Thesis, University of Calgary, Calgary, Canada, Nov. 2005.

[2] "White paper: Bluetooth wireless technology-connecting devices wirelessly with bluetooth wireless technology," Palm mobility series, 2005.

[3] "White paper: Ultra wideband: High speed, short-range technology with far-reaching effects," MBOA-SIG, Sep. 2004.

[4] "White paper: Ultra wideband technology: Enabling high-speed wireless personal area networks," Intel, Mar. 2005.

[5] J. H. Winters, "The impact of antenna diversity on the capacity of wireless communication systems," *IEEE Transactions on Communications*, vol. 42, no. 4, pp. 1740–1751, Apr. 1994.

[6] ——, "Optimum combining in digital mobile radio with cochannel interference," *IEEE Journal on Selected Areas in Communications*, vol. 2, no. 4, pp. 528–539, Jul. 1984.

[7] A. R. Calderbank, G. Pottie, and N. Seshadri, "Cochannel interference suppression through time/space diversity," *IEEE Transactions on Information Theory*, vol. 46, no. 3, pp. 922–932, May 2000.

[8] A. Paulraj, R. Nabar, and D. Gore, *Introduction to Space-Time Wireless Communications*, 1st ed. 40 West 20th Street, New York, NY, USA: Cambridge University Press, 2003.

[9] T. W. Barrett, "History of ultrawideband (uwb) radar and communications: Pioneers and innovators," in *Proc. Progress in Electromagnetics Symposium (PIERS) 2000*, Cambridge, MA, Jul. 2000.

[10] J. H. Reed, *An Introduction to Ultra Wideband Communication Systems*, 1st ed. Upper Saddle River, NJ, USA: Prentice Hall PTR, 2005.

[11] "Voluntary report-canada, doc no: Telwg32/plen/04," APEC Telecommunications and information working group, 32nd meeting, Seoul, Korea, Sep. 2005.

[12] L. Yang and G. B. Giannakis, "Ultra-wideband communications: an idea whose time has come," *IEEE Signal Processing Magazine*, vol. 21, no. 6, pp. 26–54, Nov 2004.

[13] H. Yanikomeroglu and E. S. Sousa, "Antenna gain against interference in CDMA macrodiversity systems," *IEEE Transactions on Communications*, vol. 50, no. 8, pp. 1356–1371, Aug. 2002.

[14] S. Roy and D. D. Falconer, "The matched-filter bound on optimal space-time processing in correlated fading channels," *IEEE Transactions on Wireless Communications*, vol. 3, no. 6, pp. 2156–2169, Nov. 2004.

[15] G. Zhu, "On the signalling length in digital wireless communications," M.Sc.E. Thesis, University of New Brunswick, Fredericton, Canada, September 2005.

[16] K. Gentile, "The care and feeding of digital, pulse-shaping filters," *RF Design magazine*, pp. 50–61, Apr. 2002.

[17] J. G. Proakis, *Digital Communications*, 3rd ed. New York, NY, USA: McGraw-Hill, 1995.

[18] S. Verdú, "Optimum multiuser asymptotic efficiency," *IEEE Trans. Commun.*, vol. COM-34, no. 9, pp. 890–897, Sept. 1986.

[19] N. Seshadri, "Joint data and channel estimation using blind trellis search techniques," *IEEE Trans. Commun.*, vol. 42, no. 2/3/4, pp. 1000–1011, Feb./Mar./Apr. 1994.

[20] A. Duel-Hallen, J. Holtzman, and Z. Zvonar, "Multiuser detection for cdma systems," *IEEE Personal Communications*, vol. 2, no. 2, pp. 46–58, Apr. 1995.

[21] S. Chen, A. Livingstone, and L. Hanzo, "Minimum bit-error rate design for spacetime equalization-based multiuser detection," *IEEE Transactions on Communications*, vol. 54, no. 5, pp. 824–832, May 2006.

[22] D. D. Falconer, A. Legnain, and S. Roy, "Receiver spatial-temporal signal processing for broadband wireless systems," in *The 11th IEEE International Symposium on Personal, Indoor and Mobile Radio Communications (PIMRC 2000)*, vol. 1, London, UK, Sep. 2000, pp. 676–682.

[23] M. M. Pekiner, "Convergence properties of fractionally-spaced equalizers for data transmission," M.Eng. Thesis, McGill University, Montreal, Canada, Aug. 1982.

[24] S. Qureshi, "Adaptive equalization," *IEEE Communications Magazine*, vol. 20, no. 2, pp. 9–16, Mar. 1982.

[25] G. Ungerboeck, "Fractional tap-spacing equalizer and consequences for clock recovery in data modems," *IEEE Transactions on Communications*, vol. 24, no. 8, pp. 856–864, Aug. 1976.

[26] R. D. Gitlin and S. B. Weinstein, "Fractionally-spaced equalization: An improved digital transversal equalizer," *Bell System Tech. J.*, vol. 60, no. 2, pp. 275–296, Feb. 1981.

[27] T. S. Rappaport, *Wireless Communications*. Upper Saddle River, NJ, USA: Prentice Hall PTR, 1996.

[28] W. C. Jakes, Ed., *Microwave Mobile Communications*. 445 Hoes Lane, Piscataway, NJ, USA: IEEE Press, 1993.

[29] M. Z. Win and R. A. Scholtz, "Characterization of ultra-wide bandwidth wireless indoor channels: a communication-theoretic view," *IEEE Journal on Selected Areas in Communications*, vol. 20, no. 9, pp. 1613–1627, Dec. 2002.

[30] R. A. Scholtz, R. J.-M. Cramer, and M. Z. Win, "Evaluation of the propagation characteristics of ultra-wideband communication channels," *IEEE Antennas and Propagation Society International Symposium*, vol. 2, pp. 626–630, Jun. 1998.

[31] M. A. Peyrot-Solis, G. M. Galvan-Tejada, and H. Jardon-Aguilar, "State of the art in ultra-wideband antennas," in *2nd International Conference on Electrical and Electronics Engineering*, Sep. 2005, pp. 101–105.

[32] J. Powell and A. Chandrakasan, "Antenna design for 3.1-10.6 GHz ultra wideband communication," MScE Thesis, Massachusetts Institute of Technology, 50 Vassar St. Rm 38-107, Cambridge, MA 02139, May 2004.

[33] J. Liang, C. C. Chiau, X. Chen, and C. G. Parini, "Printed circular disc monopole antenna for ultra wideband applications," *IEEE Electronics Letters*, vol. 40, no. 20, pp. 1246–1247, Sep. 2004.

[34] J. R. Foerster, M. Pendergrass, and A. F. Molisch, *A Channel Model for Ultra Wideband Indoor Communication*, Mitsubishi Electric Research Laboratory, Oct. 2003.

[35] W. C. Y. Lee, "Antenna spacing requirement for a mobile radio basestation diversity," *Bell System Tech. J.*, vol. 50, no. 6, pp. 1859–1874, Jul.-Aug. 1971.

[36] ——, "Effects on correlation between two mobile radio base-station antennas," *IEEE Transactions on Communications*, vol. 21, no. 11, pp. 1214–1224, Nov. 1973.

Appendix A

Appendix

A.1 MATLAB® programs

```
function [t1,imp,f_samp]=VNA_to_passband(rea,img)

%%%%%%%%%%%%%%%%%%%%%%%%%%%%%%%%%%%%%%%%%%%%%%%%%%%%%%%%%%%%%%%%%%%%%%%
% This function is for obtaining the real passband impulse response
% in time domain from VNA real and imaginary values of S12 or S21.
%
% Author: Nagesh Polu.
% Date Created: Nov 27,2005
% Date Modifed: April 7, 2006

% Reason for modification: Change in VNA data from 3 GHz to 7 GHz.

% Reference:
%
% Application Note AN-16a:Time Domain Spectrum Analyzer and "S"
% Parameter Vector Network Analyzer, James R. Andrews, Ph.D.,
```

```
% IEEE Fellow PSPL Founder & former President (retired)
%
*****************************************************************

  s12 = rea( : ,2 ) + i*img( : ,2 );
  freq = rea( : ,1 );
  df = freq( 2 ) - freq( 1 );
  f_bef = [ 0 : df : 3.0000e9-df ];
  f_pos = [ f_bef';  freq ];
  data_zeros = zeros( length( f_bef' ) , 1) \\
               + i * zeros( length( f_bef' ) , 1);
  data_pos = [ data_zeros ; s12 ];

% Creating window
% W=hanning(length(data_positive));

% Creative data for negative frequencies, which is the complex
% conjugate of positive frequencies data.

  data_neg = flipud(conj(data_pos(2:length(data_pos),1)));

% This section is to make the length to 2 powers, because FFT
% operates good on 2 powers.

  final_data = [ data_neg ; data_pos ];
  data_n = [ zeros(648,1) ; data_neg ];
  data_p = [ data_pos ; zeros(647,1) ];
```

```
  pr_final = [ data_p ; data_n ];

% ts=1/fs;

  N = length( pr_final );
  f_samp = N*df;
  fs = f_samp
  F = [ -fs/2 + (fs/4096) : fs/(4096) : fs/2];

  t = [ -N/2 : 1 : ( N/2 ) - 1 ] ./ fs;
  t1 = [ 0 : 1 : N - 1 ] / ( N*df );

% Real Passband Impulse response is the IFFT of passband frequency
% response

  imp = real ( ifft ( pr_final ) );
```

Vita

Candidate's full name: Veera Venkata Siva Nagesh Polu

University attended: Jawaharlal Nehru Technological University, B. Tech., 2004.

Publications:

- V. V. S. Nagesh Polu, Bruce G. Colpitts and Brent R. Petersen, "Symbol-wavelength MMSE gain in a multi-antenna UWB system," *in IEEE Proceedings of the* 4^{th} *Annual Communications Networks and Services Research Conference (CNSR 2006)*, (Moncton, NB, Canada), May 23-25, 2006, pp. 95-99.